

Latency-Response Theory Model: Evaluating Large Language Models via Response Accuracy and Chain-of-Thought Length

Zhiyu Xu¹, Jia Liu¹, Yixin Wang², and Yuqi Gu^{*1}

¹Department of Statistics, Columbia University.

²Department of Statistics, University of Michigan

Abstract

The proliferation of Large Language Models (LLMs) necessitates valid evaluation methods to provide guidance for both downstream applications and actionable future improvements. The Item Response Theory (IRT) model with Computerized Adaptive Testing has recently emerged as a promising framework for evaluating LLMs via their response accuracy. Beyond simple response accuracy, LLMs’ chain of thought (CoT) lengths serve as a vital indicator of their reasoning ability. To leverage the CoT length information to assist the evaluation of LLMs, we propose the **Latency-Response Theory** (LaRT) model, which jointly models both the response accuracy and CoT length by introducing a key correlation parameter between the latent ability and the latent speed. We derive an efficient stochastic approximation Expectation-Maximization algorithm for parameter estimation. We establish rigorous identifiability results for the latent ability and latent speed parameters to ensure the statistical validity of their estimation. Through both theoretical asymptotic analyses and simulation studies, we demonstrate LaRT’s advantages over IRT in terms of superior estimation accuracy and shorter confidence intervals for latent trait estimation. To evaluate LaRT in real data, we collect responses from diverse LLMs on popular benchmark datasets. We find that LaRT yields different LLM rankings than IRT and outperforms IRT across multiple key evaluation metrics including predictive power, item efficiency, ranking validity, and LLM evaluation efficiency. Code and data are available at <https://github.com/Toby-X/Latency-Response-Theory-Model>.

Keywords: Large language models, Chain of thought, Item response theory, Identifiability, Stochastic Approximation

1 Introduction

As large language models (LLMs) continue to advance across diverse tasks, it has become increasingly crucial to effectively and reliably evaluate their abilities (Liang et al., 2023). A common approach to evaluating an LLM’s capability is using a corresponding benchmark, such as GSM8K for mathematical reasoning (Cobbe et al., 2021), HumanEval for code generation (Chen, 2021), or MMLU for general knowledge reasoning. The LLM is run on the benchmark items, its outputs are scored using task-specific metrics, and the resulting score is used to compare or rank LLMs. However, benchmark scores alone provide only a coarse measure of performance and offer limited insight into how or why LLMs differ, as they do not account for variation in item characteristics or model-specific response patterns.

*{zx2488,jl6795}@columbia.edu; yixinw@umich.edu; yuqi.gu@columbia.edu. Corresponding author: Yuqi Gu.

Recently, Item Response Theory (IRT), together with Computerized Adaptive Testing (CAT), from the psychometrics literature has emerged as a promising framework for evaluating LLMs in a more principled and interpretable manner (Lalor et al., 2016; Zhuang et al., 2023; Maia Polo et al., 2024; Kipnis et al., 2025; Castleman et al., 2025; Hofmann et al., 2025). Unlike raw benchmark scoring, which treats all items as equally informative, IRT explicitly models variation in item difficulty and discrimination and therefore provides a latent ability estimate that is comparable across models and datasets. In this context, IRT can be used in two complementary ways. First, in a *static evaluation setting*, IRT is applied to existing benchmark responses to estimate each model’s latent ability and to produce model rankings. Second, IRT can also support an *active evaluation setting*, where item parameters are first estimated from a pool of problems and then used to infer a model’s ability based on selectively chosen items (Ein-Dor et al., 2020). This enables tracking how a model’s ability evolves during training or under limited evaluation budgets, and closely relates to CAT procedures that aim to estimate ability efficiently by administering only the most informative items (Chang and Ying, 1996).

Existing IRT-based evaluations of LLMs consider only the final response outcome. Yet, the response-generation process inherently contains information about the model’s reasoning behavior. In particular, *chain of thought* (CoT) is a vital indicator of reasoning in LLMs. Wei et al. (2022) demonstrated that prompts eliciting CoT reasoning significantly enhance LLMs’ ability to resolve complex task. Given the autoregressive nature of LLMs, extending the CoT length necessitates additional decoding steps, thereby increasing the computation at test time. Snell et al. (2025) discovered that scaling the test-time compute via extending CoT length is often more effective than scaling model parameters. Consequently, recent training strategies for reasoning models prioritize extended CoT generation. For instance, Deepseek-R1 targets longer CoT sequences in training to improve performance (Guo et al., 2025). OpenAI’s o1 similarly emphasizes eliciting CoT during training (Jaech et al., 2024). Therefore, CoT length can serve as a process-level indicator of how much intermediate reasoning the model performs prior to producing an answer. Incorporating both accuracy and CoT length into a unified modeling and evaluation framework can therefore yield more reliable and discriminative ability estimates, which motivates this work. CoT length closely parallels the role of response time (RT) in student assessment, where the duration of problem solving is used as an auxiliary indicator of cognitive effort beyond correctness alone (e.g., van der Linden, 2007; Meng et al., 2015; Klein Entink et al., 2009).

The joint modeling of response accuracy and response time has been studied in psychometrics (see Schnipke and Scrams, 2005; De Boeck and Jeon, 2019; Kyllonen and Zu, 2016, for overviews). Foundational work conceptualized response time as an indicator of cognitive processing effort (Luce, 1991; Schnipke and Scrams, 2005), and subsequent developments have proposed a range of cognitive process modeling approaches, including hierarchical joint IRT–RT models (van der Linden, 2007), evidence-accumulation models such as the drift diffusion model (DDM; Van Der Maas et al., 2011), and competitive race formulations (Rouder et al., 2015). Among these approaches, the hierarchical IRT–RT framework is particularly suitable for our setting. Whereas evidence-accumulation and race models impose specific assumptions on the form of the underlying reasoning process, the hierarchical approach does not commit to a particular cognitive mechanism and instead treats response time as an observable process signal linked to latent traits. This leads to a more flexible and assumption-light measurement framework.

Despite these developments, existing methodologies in psychometrics face limitations that hinder their direct application to LLM evaluation. From a statistical perspective, these models *lack strict theoretical identifiability guarantees*. Identifiability ensures that no two distinct parameter configurations yield the same marginal distribution of observed data, and it is essential for consistency, interpretability, and reliable parameter recovery. From a computational perspective, existing

models are typically *computationally expensive*, hence difficult to scale to LLM evaluation settings, where benchmark datasets typically contain a large number of items: they often estimate the joint models using Markov chain Monte Carlo (MCMC; e.g. [Fox and Mariani 2016](#); [Bolsinova and Tjmsstra 2019](#)) algorithms due to the intractable marginal likelihood function involving complicated integrals. Yet, MCMC-based estimation is computationally intensive, as each iteration requires repeatedly sampling latent traits and item parameters across all items, leading to slow convergence when the item pool is large. Alternative approaches like EM-based estimation also involve evaluating likelihood terms that aggregate information over many items, making the numerical integration step progressively more expensive as the number of items increases. Consequently, both approaches struggle to scale to benchmark datasets with large item pools.

This article makes the following contributions. *First*, we propose an identifiable Latency–Response Theory (LaRT) model through jointly modeling response accuracy and chain-of-thought length. LART introduces a key correlation parameter $\rho \in (-1, 1)$ between latent ability and the latent speed, allowing the two signals to complement one another in estimating model proficiency. We establish rigorous identifiability guarantees for LaRT. These results are crucial to trustworthy LLM evaluation, ensuring reliable inference while laying a solid foundation for potential extensions to other joint modeling scenarios. We demonstrate the benefits of this joint modeling approach through both theoretical asymptotic analysis and simulation studies. Theoretically, we illustrate that LaRT yields shorter confidence intervals for latent trait estimation compared to IRT for a fixed sample size. In simulation studies, LaRT achieves significantly higher estimation accuracy than IRT across all model parameters.

Second, we develop an efficient stochastic approximation Expectation-Maximization (SAEM) algorithm to estimate population parameters and individual latent traits of the LLMs. To adapt SAEM to the LaRT setting, we develop tailored implementation strategies that ensure both computational efficiency and algorithmic stability. Specifically, to accelerate each SAEM iteration, we design an effective latent-trait sampler that avoids MCMC. Leveraging the probit link and recent analytical results for probit models with normal priors ([Durante, 2019](#)), we show that the latent traits admit a simple two-step sampling scheme based solely on efficient normal and truncated-normal draws ([Li et al., 2025](#)). Further, we introduce a fast spectral initialization that enhances estimation quality and stability. This method extends the SVD-based procedure of [Zhang et al. \(2020\)](#) to the multimodal response-accuracy/CoT setting by adding CoT-specific steps under the LaRT hierarchy. This initialization procedure avoids the burn-in phase of classical SAEM and substantially reduces the number of required iterations. After estimating the population parameters, individual latent traits are obtained via maximum-a-posteriori (MAP) estimation, which reduces to convex optimization problems.

Third, to evaluate LaRT in practical settings, we conduct comprehensive empirical data analysis on real data by collecting responses from diverse LLMs on popular benchmark datasets. We observe an interpretable and consistent trend across all benchmark datasets: LLMs with greater latent ability exhibit lower latent speed (longer CoT). Quantitatively, we compare the performance of LaRT against IRT on the real-world data. We find that LaRT yields different model rankings than IRT. Moreover, LaRT outperforms IRT across multiple key evaluation metrics in LLM evaluation: *predictive power* (prediction accuracy on unseen question items), *validity* (ranking consistency over different benchmark datasets), *item efficiency* (the number of items required for evaluation), and *LLM efficiency* (the number of LLMs required for evaluation).

The rest of this paper is organized as follows. Section 2 introduces the Latency–Response Theory model. Section 3 presents an efficient SAEM algorithm with data-driven initialization for estimating population parameters, and a Maximum-A-Posterior algorithm to estimate the latent traits. Section 4 presents the identifiability results for LaRT and the asymptotic distribution of the latent traits.

In Section 5, we perform simulations to validate the performance of our proposed methodology. Finally, Section 6 applies LaRT to real-world LLM evaluation settings, offering a comprehensive qualitative and quantitative comparison against standard IRT models across multiple performance dimensions. Section 7 concludes and discusses future directions.

2 Latency-Response Theory Model (LaRT)

2.1 Notation

We introduce some notations used throughout this paper. Denote the response accuracy matrix as $\mathbf{R} = (R_{ij}) \in \{0, 1\}^{N \times J}$, collecting responses of N LLMs to J test questions, where $R_{ij} = 1$ or 0 indicates whether LLM i answers question j correctly or not. Denote the CoT length matrix as $\mathbf{T} = (T_{ij}) \in \mathbb{N}_+^{N \times J}$, where T_{ij} is a positive number recording the CoT length when LLM i responds to question j . Denote the $K \times K$ identity matrix as \mathbf{I}_K . Standard multivariate Gaussian probability density function of K dimensions is denoted as $\phi_K(\mathbf{x})$, and its cumulative density function is denoted as $\Phi_K(\mathbf{x})$. When $K = 1$, we omit the subscript K . Additionally, for a random variable $\mathbf{X} \sim N(\mathbf{0}_K, \mathbf{I}_K)$, for a set $B \in \mathbb{R}^K$, we denote $\tilde{\Phi}(B) = P(\mathbf{X} \in B)$. Let $[K] = \{1, 2, \dots, K\}$ for any non-negative integer K .

2.2 The LaRT Framework

We propose a hierarchical LaRT framework that jointly models response accuracy and CoT variables. In this framework, the binary response accuracy is modeled using an item response model with a probit link, while CoT is modeled through a log-normal distribution with a latent speed variable. The subject-level latent traits underlying these two components are jointly specified by a two-dimensional multivariate normal distribution, where the correlation captures the dependence between latent traits. This model specifications draw inspirations from hierarchical frameworks in psychometrics that jointly model response accuracy and response time (van der Linden, 2007; Entink et al., 2009; Wang and Xu, 2015), while being motivated by the parallel role of CoT processes and response times as indicators of intermediate reasoning.

$$R_{ij} \sim \text{Bernoulli}(\Phi(a_j\theta_i + b_j)), \quad (1a)$$

$$\log T_{ij} \sim N(\omega_j - \varphi_j\tau_i, \lambda_j), \quad (1b)$$

$$(\theta_i, \tau_i)^\top \sim N(0, \Sigma), \quad (1c)$$

$$\Sigma = \begin{pmatrix} 1 & \rho \\ \rho & 1 \end{pmatrix}, \quad (1d)$$

In the IRT model in (1a), θ_i denotes the latent ability of LLM i , representing its position on the underlying proficiency scale. The discrimination parameter a_j describes how strongly item j differentiates between LLMs with different ability levels. The parameter b_j represents the difficulty of item j , with smaller values indicating more difficult items, i.e. items that require higher ability for a correct response. Among the two commonly used link functions for IRT models (the logit link and the probit link), we employ the latter, as its desirable mathematical properties support developing both theoretical identifiability results and computational estimation methods, as detailed later in Sections 3 and 4.1.

In (1b), we use a log-normal distribution to model the length of CoT. Here, τ_i denotes a latent speed variable representing the CoT-related trait of LLM i . ω_j represents the CoT-intensity of

item j , with larger values indicating items that require more intermediate reasoning. The coefficient φ_j reflects the CoT-discrimination of item j , measuring the sensitivity of CoT lengths to differences in LLMs’ latent speed τ_i . λ_j is the residual variance of the log-CoT ($\log T_{ij}$). The use of log-normal distribution for CoT length is justified by both empirical observations and theoretical considerations. Empirically, CoT lengths produced by LLMs are typically large (often in the range of hundreds to thousands), and in our applications fewer than 1% of the CoT are shorter than 10. Theoretically, the log-normal distribution serves as an asymptotic approximation to common count distributions, such as the Poisson and negative binomial, when the counts are large. Thus, for large T_{ij} , the log-normal is a suitable choice for modeling CoT length. Moreover, as shown later, this specification offers mathematical conveniences that, together with the probit link, support rigorous identifiability analysis and efficient estimation algorithms.

Finally, in Equations (1c)-(1d), the diagonal entries of Σ are fixed to 1 to identify the scale of the latent traits, and the off-diagonal entry of Σ is denoted by ρ , so that Σ is essentially a correlation matrix. We provide theoretical identifiability results in Section 4.1. For notational simplicity, we denote the collection of population parameters (i.e., parameters not depending on individual LLMs) by $\Omega = \{\mathbf{a}, \mathbf{b}, \boldsymbol{\omega}, \boldsymbol{\varphi}, \boldsymbol{\lambda}, \rho\}$.

3 Estimation Algorithm

Parameter estimation is crucial for applying the LaRT framework to LLM evaluation. The main estimation challenge for the population parameters arises from the intractability of the observed-data likelihood:

$$P(\mathbf{R}, \mathbf{T}; \Omega) = \int \prod_{i=1}^N \prod_{j=1}^J \left[\Phi((2R_{ij} - 1)(a_j\theta_i - b_j)) \frac{1}{\sqrt{2\pi\lambda_j}} \exp \left\{ -\frac{1}{2\lambda_j} (\log T_{ij} - \omega_j + \varphi_j\tau_i)^2 \right\} \right] \prod_{i=1}^N \frac{1}{2\pi(1-\rho^2)^{1/2}} \exp \left\{ -\frac{1}{2} \boldsymbol{\xi}_i^\top \Sigma^{-1} \boldsymbol{\xi}_i \right\} d\boldsymbol{\theta} d\boldsymbol{\tau} \quad (2)$$

Direct likelihood maximization is computationally infeasible because Equation (2) requires evaluating a high-dimensional integral over the latent variables $(\boldsymbol{\theta}, \boldsymbol{\tau})$. As a potential solution, the Expectation–Maximization (EM) algorithm replaces the intractable observed-data likelihood with the expected complete-data log-likelihood. By iteratively computing this expectation and maximizing it, EM transforms the original optimization into a sequence of tractable updates. However, the E-step requires computing conditional expectations that also involves intractable integrals. Stochastic Approximation EM (Delyon et al., 1999, SAEM) solves this second intractability by replacing the intractable conditional expectation with Monte Carlo approximations updated through a Robbins–Monro stochastic approximation scheme (Robbins and Monro, 1951), thereby avoiding explicit integration while preserving the EM structure.

While SAEM has been widely used in latent variable modeling, its successful application to LaRT requires three additional model-specific components that tailor implementation strategies to ensure computational efficiency and algorithmic stability: (1) an efficient sampler for the latent variables that can substantially improve both computational speed and convergence behavior, (2) a suitable initialization strategy that can reduce the number of iterations and enhance estimation accuracy, and (3) a method for estimating individual LLM latent variables after obtaining population parameters. This section develops each component in turn. We first propose an efficient SAEM algorithm for estimating the population parameters of LaRT in Subsection 3.1, addressing the aspects discussed above. Next, in Subsection 3.2, we introduce an effective spectral-based ini-

tialization method for the proposed SAEM. Finally, in Subsection 3.3, we describe how to estimate the latent variables of LLMs once the population parameters have been obtained, under both static and active evaluation settings.

3.1 SAEM Algorithm for Population Parameter Estimation

The SAEM algorithm addresses the intractable E-step of EM through a stochastic approximation scheme. It alternates three steps: at each iteration, latent variables are sampled in an S-step and used to approximate the conditional expectation in an SA-step, followed by an M-step that updates the population parameters. The SAEM steps operates on the following complete-data log-likelihood:

$$\begin{aligned}
L(\boldsymbol{\Omega}, \boldsymbol{\theta}, \boldsymbol{\tau} \mid \mathbf{R}, \mathbf{T}) &= \log P(\mathbf{R} \mid \boldsymbol{\theta}; \boldsymbol{\Omega}) + \log P(\mathbf{T} \mid \boldsymbol{\tau}; \boldsymbol{\Omega}) + \log P(\boldsymbol{\theta}, \boldsymbol{\tau}; \boldsymbol{\Omega}) \\
&= \sum_{i=1}^N \sum_{j=1}^J \log \Phi((2R_{ij} - 1)(a_j \theta_i + b_j)) - N \sum_{j=1}^J \log \lambda_j \\
&\quad - \sum_{i=1}^N \sum_{j=1}^J \frac{1}{2\lambda_j^2} (\log T_{ij} - \omega_j + \varphi_j \tau_i)^2 - \frac{N}{2} \log(1 - \rho^2) - \frac{1}{2} \sum_{i=1}^N \boldsymbol{\xi}_i^\top \boldsymbol{\Sigma}^{-1} \boldsymbol{\xi}_i.
\end{aligned} \tag{3}$$

Next, we introduce the three steps separately and describe their detailed derivation and implementation.

S-step. The S-step requires drawing samples of the LLM latent variables (θ_i, τ_i) from their posterior distribution given the data and the current population parameters:

$$\begin{aligned}
P(\theta_i, \tau_i \mid \mathbf{R}_{i,:}, \mathbf{T}_{i,:}; \boldsymbol{\Omega}) &\propto P(\theta_i, \tau_i; \boldsymbol{\Omega}) \prod_{j=1}^J P(R_{ij} \mid \theta_i; \boldsymbol{\Omega}) P(T_{ij} \mid \tau_i; \boldsymbol{\Omega}) \\
&= \left[P(\theta_i; \boldsymbol{\Omega}) \prod_{j=1}^J P(R_{ij} \mid \theta_i; \boldsymbol{\Omega}) \right] \left[P(\tau_i \mid \theta_i; \boldsymbol{\Omega}) \prod_{j=1}^J P(T_{ij} \mid \tau_i; \boldsymbol{\Omega}) \right].
\end{aligned} \tag{4}$$

Direct joint sampling of (θ_i, τ_i) from (4) is infeasible. Fortunately, LaRT’s structure, specifically the probit link for response accuracy and the log-normal model for CoT, enables an efficient two-step sampling procedure that avoids MCMC-based samplers such as Metropolis–Hastings or Gibbs. In particular, because both the conditional prior $P(\tau_i \mid \theta_i; \boldsymbol{\Omega})$ and the likelihood $P(T_{ij} \mid \tau_i; \boldsymbol{\Omega})$ are normal, the conditional posterior $P(\tau_i \mid \theta_i, \mathbf{T}_{i,:}; \boldsymbol{\Omega})$ also remains normal. Thus, once a sample of θ_i is obtained, τ_i can be drawn directly from a normal distribution. The remaining task is thus to sample θ_i from its marginal posterior $P(\theta_i \mid \mathbf{R}_{i,:}, \boldsymbol{\Omega})$, obtained by integrating out τ_i in (4). Benefiting from the structure induced by the probit likelihood and Gaussian prior, this marginal posterior falls within the family of unified skew-normal (SUN) distributions. Leveraging the analytical characterization developed in Durante (2019), we explicitly characterize its posterior distribution, as presented in the following lemma.

Lemma 1. *The posterior distribution of (θ_i, τ_i) given \mathbf{R} , \mathbf{T} , and $\boldsymbol{\Omega}$ follows the following distribution,*

$$\theta_i \mid \mathbf{R}; \boldsymbol{\Omega} \sim \text{SUN}_{1,J} \left(\mu_\theta^{(i)}, \sigma_\theta^2, \Delta_{i,\text{post}}, \gamma_{i,\text{post}}, \Gamma_{i,\text{post}} \right) \tag{5}$$

$$\tau_i \mid \theta_i, \mathbf{T}; \boldsymbol{\Omega} \sim N \left(\boldsymbol{\mu}_\tau^{(i)}, \sigma_\tau^2 \right), \tag{6}$$

where SUN represents the unified skew-normal distribution, and

$$\begin{aligned}\sigma_\tau^2 &= \left(\frac{1}{1-\rho} + \sum_{j=1}^J \frac{\varphi_j^2}{\lambda_j} \right)^{-1}, \quad \mu_\tau^{(i)} = \frac{\rho\theta_i}{1-\rho^2} - \sum_{j=1}^J \frac{(\log T_{ij} - \omega_j)\varphi_j}{\lambda_j}, \\ \sigma_\theta^2 &= \left(\frac{1}{1-\rho^2} - \sigma_\tau^2 \frac{\rho^2}{1-\rho^2} \right)^{-1}, \quad \mu_\theta^{(i)} = \sigma_\theta^2 \left(- \sum_{j=1}^J \frac{(\log T_{ij} - \omega_j)\varphi_j}{\lambda_j} \right) \frac{\sigma_\tau^2 \rho}{1-\rho^2} \\ \Delta_{i,\text{post}} &= \sigma_\theta \mathbf{D}_{i,1}^\top \mathbf{S}_i^{-1}, \quad \gamma_{i,\text{post}} = \mathbf{S}_i^{-1} \left(\mathbf{D}_{i,1} \mu_\theta^{(i)} + \mathbf{D}_{i,2} \right), \\ \Gamma_{i,\text{post}} &= \mathbf{S}_i^{-1} \left(\sigma_\theta^2 \mathbf{D}_{i,1} \mathbf{D}_{i,1}^\top + \mathbf{I}_J \right) \mathbf{S}_i^{-1},\end{aligned}$$

and

$$\begin{aligned}\mathbf{D}_{i,1} &= \text{diag}(2R_{i1} - 1, \dots, 2R_{iJ} - 1) \mathbf{a}, \quad \mathbf{D}_{i,2} = \text{diag}(2R_{i1} - 1, \dots, 2R_{iJ} - 1) \mathbf{b}, \\ \mathbf{S}_i &= \text{diag} \left\{ (\sigma_\theta^2 \mathbf{D}_{i,11}^\top \mathbf{D}_{i,11} + 1)^{1/2}, \dots, (\sigma_\theta^2 \mathbf{D}_{i,1J}^\top \mathbf{D}_{i,1J} + 1)^{1/2} \right\} \in \mathbb{R}^{J \times J},\end{aligned}$$

where $\mathbf{D}_{i,1,j}$ is the j th row of $\mathbf{D}_{i,1}$.

Lemma 1 provides the explicit distributional expressions discussed above for sampling θ_i and τ_i . Furthermore, the SUN distribution can be sampled efficiently, as stated in the following corollary from Li et al. (2025). Taken together, these results yield the proposed efficient sampler for the S-step.

Corollary 1 (Corollary 4.3 in Li et al. (2025)). *If (θ_i, τ_i) follows the distribution specified in Lemma 1, then*

$$\theta_i \mid \mathbf{R}_{i,:}; \boldsymbol{\Omega} \stackrel{d}{=} \mu_\theta^{(i)} + \sigma_\theta \left[U_0 + \sigma_\theta \mathbf{D}_{i,1}^\top \left(\sigma_\theta^2 \mathbf{D}_{i,1} \mathbf{D}_{i,1}^\top + \mathbf{I}_J \right)^{-1} \mathbf{S} U_1 \right], \quad (7)$$

where $U_0 \sim N\left(0, 1 - \sigma_\theta^2 \mathbf{D}_{i,1}^\top (\sigma_\theta^2 \mathbf{D}_{i,1} \mathbf{D}_{i,1}^\top + \mathbf{I}_J)^{-1} \mathbf{D}_{i,1}\right)$, U_1 follows a truncated normal distribution with mean 0 and variance $\mathbf{S}^{-1} (\sigma_\theta^2 \mathbf{D}_{i,1} \mathbf{D}_{i,1}^\top + \mathbf{I}_J) \mathbf{S}^{-1}$, truncated with lower bound at $-\mathbf{S}^{-1} (\mathbf{D}_{i,1} \mu_\theta^{(i)} + \mathbf{D}_{i,2})$, and U_0 is independent of U_1 .

Taken together, these results yield a two-step sampler for (θ_i, τ_i) . First, θ_i is drawn from the SUN distribution in (5), which can be implemented via a linear combination of samples from a multivariate normal distribution and a truncated normal distribution, as in (7). Second, τ_i is then sampled from the normal distribution in (6). Since all target distributions admit straightforward sampling, the S-step can be implemented efficiently.

SA-step. The SA-step updates the current estimate of the conditional expectation of the log complete posterior using a stochastic approximation scheme. At each iteration t , it first uses the C samples of (θ_i, τ_i) , denoted by $\boldsymbol{\xi}_i^{(c)} = (\theta_i^{(c)}, \tau_i^{(c)})$, $c \in [C]$, obtained in the S-step to form a Monte Carlo approximation of this conditional expectation:

$$\begin{aligned}Q_t^{(\text{new})}(\boldsymbol{\Omega}) &= \frac{1}{C} \sum_{c=1}^C \sum_{i=1}^N \sum_{j=1}^J \log \Phi \left((2R_{ij} - 1)(a_j \theta_i^{(c)} + b_j) \right) - N \sum_{j=1}^J \log \lambda_j \\ &\quad - \frac{1}{C} \sum_{c=1}^C \sum_{i=1}^N \sum_{j=1}^J \frac{1}{2\lambda_j^2} (\log T_{ij} - \omega_j + \varphi_j \tau_i^{(c)})^2 \\ &\quad - \frac{N}{2} \log(1 - \rho^2) - \frac{1}{2C} \sum_{c=1}^C \sum_{i=1}^N \boldsymbol{\xi}_i^{(c)\top} \boldsymbol{\Sigma}^{-1} \boldsymbol{\xi}_i^{(c)}.\end{aligned} \quad (8)$$

The constant C denotes the number of Monte Carlo samples drawn at each SA-step. Although a larger C can reduce Monte Carlo variability, it also increases computational cost. Following standard SAEM practice, we set $C = 1$, which is sufficient for stable estimation in our setting. Then, this Monte Carlo estimate is incorporated into the running approximation of the conditional expectation through a Robbins–Monro stochastic approximation update:

$$\tilde{Q}_t(\boldsymbol{\Omega}) = (1 - \alpha_t) \tilde{Q}_{t-1}(\boldsymbol{\Omega}) + \alpha_t Q_t^{(\text{new})}(\boldsymbol{\Omega}),$$

with initialization $\tilde{Q}_1(\boldsymbol{\Omega}) = Q_1^{(\text{new})}(\boldsymbol{\Omega})$. As shown, the new estimate $\tilde{Q}_t(\boldsymbol{\Omega})$ is a weighted mixture of the current Monte Carlo estimate $Q_t^{(\text{new})}(\boldsymbol{\Omega})$ and the previous estimate $\tilde{Q}_{t-1}(\boldsymbol{\Omega})$. The sequence $\{\alpha_t\}$ denotes the step sizes and is required to satisfy the Robbins–Monro conditions $\sum_t \alpha_t = \infty$ and $\sum_t \alpha_t^2 < \infty$ to ensure convergence. A typical choice that meets these requirements is $\alpha_t = 1/t$. Through this averaging, the stochastic approximation update stabilizes the sequence of expectation estimates by weighting new updates $Q_t^{(\text{new})}(\boldsymbol{\Omega})$ with decreasing step sizes, allowing the algorithm to converge even when only a small number of samples is used at each step (Robbins and Monro, 1951; Delyon et al., 1999).

M-step. In the M-step, the population parameters are updated by maximizing the current $\tilde{Q}_t(\boldsymbol{\Omega})$. Importantly, the concavity of $Q_t^{(\text{new})}$ in $\boldsymbol{\Omega}$ is preserved under the Robbins–Monro averaging step, ensuring that Q_t remains concave and can therefore be maximized efficiently. To this end, we employ the L-BFGS algorithm (Liu and Nocedal, 1989), a widely used and efficient quasi-Newton method for smooth convex optimization, to perform the M-step at each iteration. The complete SAEM procedure is outlined in Algorithm 1.

Algorithm 1 SAEM algorithm for the estimation of population parameters.

Require: Binary response matrix $\mathbf{R} \in \{0, 1\}^{N \times J}$, CoT length matrix $\mathbf{T} \in \mathbb{R}_+^{N \times J}$, Initialization $\hat{\boldsymbol{\Omega}}_0$, Number of Monte Carlo samples C , stochastic approximation weights $\{\alpha_t\}_{t \in \mathbb{N}}$.

Ensure: Estimated $\hat{\boldsymbol{\Omega}}$.

- 1: Initialize $t \leftarrow 0$, $Q_0 \leftarrow 0$.
 - 2: **while** not converge **do**
 - 3: $t \leftarrow t + 1$.
 - 4: Draw C samples of $(\boldsymbol{\theta}^{(c)}, \boldsymbol{\tau}^{(c)})$ following Lemma 1 and Corollary 1.
 - 5: Compute $Q_t^{(\text{new})}$ by (8), and $\tilde{Q}_t \leftarrow (1 - \alpha_t) \tilde{Q}_{t-1} + \alpha_t Q_t^{(\text{new})}$.
 - 6: $\hat{\boldsymbol{\Omega}}_t \leftarrow \operatorname{argmax}_{\boldsymbol{\Omega}} \tilde{Q}_t(\boldsymbol{\Omega})$ with a valid convex optimization algorithm.
 - 7: **end while**
 - 8: Return $\hat{\boldsymbol{\Omega}}_t$.
-

3.2 Initialization for the SAEM algorithm

Effective initialization is critical for SAEM’s efficiency and stability. We present a spectral-based initialization that is non-iterative, data-driven, and statistically consistent. This approach exploits the fact that the probit link for response accuracy and the log-normal specification for CoT fall within the scope of generalized linear factor models (GLMs) or linear factor models, allowing us to adapt the spectral-based method of Zhang et al. (2020), originally developed for GLM settings, to initialize the LaRT framework. Specifically, we extend their procedure—which was designed for single-modality response-accuracy data—to accommodate the bimodal structure of response accuracy and CoT, introducing additional steps to initialize the CoT-related parameters under the

LaRT hierarchical model. Algorithm 2 summarizes the full algorithm.

Algorithm 2 Nonlinear Spectral Initialization for the SAEM algorithm.

Require: Binary response matrix $\mathbf{R} \in \{0, 1\}^{N \times J}$, CoT length matrix $\mathbf{T} \in \mathbb{R}_+^{N \times J}$, thresholding parameter $\epsilon_{N,J}$.

Ensure: Spectral estimates of $\check{\mathbf{\Omega}}, \check{\theta}_i, \check{\tau}_i$ for $i \in [N]$.

- 1: Perform a full SVD of $\mathbf{R} = \sum_{i=1}^{N \wedge J} \sigma_i \mathbf{u}_i \mathbf{v}_i^\top$.
- 2: Let $\mathbf{X} = \sum_{k=1}^{\tilde{K}} \sigma_k \mathbf{u}_k \mathbf{v}_k^\top$, where $\tilde{K} = \max\{K + 1, \operatorname{argmax}_k \{\sigma_k \geq 1.01\sqrt{N \vee J}\}\}$.
- 3: Let $\tilde{\mathbf{M}} = (\tilde{M}_{ij})_{N \times J}$ be

$$\tilde{M}_{ij} = \begin{cases} \Phi^{-1}(\epsilon_{N,J}), & \text{if } x_{ij} < \epsilon_{N,J}, \\ \Phi^{-1}(x_{ij}), & \text{if } \epsilon_{N,J} \leq x_{ij} \leq 1 - \epsilon_{N,J}, \\ \Phi^{-1}(1 - \epsilon_{N,J}), & \text{if } x_{ij} > 1 - \epsilon_{N,J}. \end{cases}$$

- 4: Let $\check{b}_j = \sum_{i=1}^N \tilde{m}_{ij}/N$, $\check{\omega}_k = \sum_{i=1}^N \log T_{ij}/N \forall j \in [J]$.
 - 5: Perform top-1 SVD on $\tilde{\mathbf{M}} = (\tilde{M}_{ij} - \check{b}_j)_{N \times J}$ and $\log \hat{\mathbf{T}} = (\log T_{ij} - \check{\omega}_j)_{N \times J}$ for respectively $\check{\sigma}_1 \check{\mathbf{u}}_1 \check{\mathbf{v}}_1^\top$ and $\check{\sigma}_1 \check{\mathbf{u}}_1 \check{\mathbf{v}}_1^\top$.
 - 6: Let $\check{\boldsymbol{\theta}} = \sqrt{N} \check{\mathbf{u}}_1$, $\check{\mathbf{a}} = \check{\sigma}_1 \check{\mathbf{v}}_1 / \sqrt{N}$, $\check{\boldsymbol{\tau}} = \sqrt{N} \check{\mathbf{u}}_1$, and $\check{\boldsymbol{\varphi}} = \check{\sigma}_1 \check{\mathbf{v}}_1 / \sqrt{N}$.
 - 7: Let $\check{\rho} = \sum_{i=1}^N \check{\theta}_i \check{\tau}_i / N$, and $\check{\lambda}_j = \sum_{i=1}^N (\log \hat{T}_{ij} - \check{\tau}_i \check{\varphi}_j)^2 / N$.
-

The algorithm proceeds in three stages. The algorithm begins by first performing an SVD on the response accuracy matrix to extract its dominant latent structure and reduce noise, followed by an inverse link transformation to obtain an approximately linear latent representation (steps 1–3). In step 3, $\epsilon_{N,J}$ serves as a threshold for truncating \mathbf{X} to the range of \mathbf{R} , and is set to 10^{-9} in this work, following the general guidelines in Zhang et al. (2020). The estimates of the difficulty parameters \check{b}_j and the intensity parameters $\check{\omega}_k$ are obtained by averaging the corresponding entries in the transformed data $\tilde{\mathbf{M}}$, respectively, as these parameters serve as intercepts in their linear factor model forms (step 4). Then, SVD is applied to the centered $\tilde{\mathbf{M}}$ and $\log(\mathbf{T})$, and the estimates of the discrimination parameters $\check{\mathbf{a}}$ and $\check{\boldsymbol{\varphi}}$, as well as the latent ability variables $\check{\boldsymbol{\theta}}$ and $\check{\boldsymbol{\tau}}$, are obtained by extracting their corresponding components from the SVD (steps 5–6). Finally, the log-CoT residual variance estimates $\check{\lambda}_j$ and the correlation estimate $\check{\rho}$ are computed using their closed-form expressions, $\sum_{i=1}^N (\log \hat{T}_{ij} - \check{\tau}_i \check{\varphi}_j)^2 / N$ and $\sum_{i=1}^N \theta_i \tau_i / N$, respectively (step 7). For more details on the implementation, please refer to Zhang et al. (2020).

This informed initialization enables the algorithm to adopt a decaying step size α_t from the very first iteration. In contrast, standard SAEM implementations typically require an initial *burn-in* phase, during which a large step size (e.g., $\alpha_t = 1$) must be used for many iterations (Lavielle and Mbogning, 2014; Kuhn and Lavielle, 2004; Camilli and Geis, 2019). This phase is crucial when using random initializations, which often start far from the optimum and therefore require large updates to move into the optimal region. However, it also introduces an additional tuning burden: the appropriate length of the burn-in phase varies with the initial values, making the procedure more unstable and sensitive to initialization. This initialization strategy bypasses this burn-in phase entirely by replacing random initialization with an efficient, non-iterative, data-driven strategy, while also enjoying favorable statistical consistency properties (Zhang et al., 2020). Our spectral initialization starts near the optimum, allowing SAEM to use a decaying step size from iteration one. This yields both faster convergence and improved estimation accuracy compared with traditional SAEM implementations, as demonstrated in Appendix D.

3.3 Maximum-a-posterior estimation for individual latent ability and speed.

After obtaining the estimates of the population parameters, we estimate the individual latent variables $(\boldsymbol{\theta}, \boldsymbol{\tau})$ based on Maximum-A-Posterior (MAP) estimation:

$$(\boldsymbol{\theta}, \boldsymbol{\tau}) = \underset{(\boldsymbol{\theta}, \boldsymbol{\tau})}{\operatorname{argmax}} L(\widehat{\boldsymbol{\Omega}}, \boldsymbol{\theta}, \boldsymbol{\tau} \mid \mathbf{R}, \mathbf{T}). \quad (9)$$

Given the population parameters $\boldsymbol{\Omega}$, the log complete posterior (3) is concave with respect to $\boldsymbol{\xi} = (\boldsymbol{\theta}, \boldsymbol{\tau})$. This observation, together with the independence across the $\boldsymbol{\xi}_i$'s, reduces the optimization problem to N convex optimization problems with two-dimensional parameters, each of which can be solved efficiently using L-BFGS.

Finally, the proposed estimation procedure for population parameters and individual latent traits applies to both static and active evaluation settings. In static evaluation, the population parameters are first estimated by applying SAEM to fit a LaRT model to the LLM response data, after which the MAP estimates of the LLMs' latent traits are obtained by solving (9). In active evaluation, LLMs are administered a set of items drawn from a calibrated item pool, where the items can be calibrated using an appropriate estimator such as the proposed SAEM. As each LLM answers items, we update its latent trait estimates by solving (9) with the current response data.

4 Theoretical Results

In this section, we present theoretical results for LaRT. First, we prove identifiability to ensure statistical validity of inferences about LLM latent traits. Second, we derive asymptotic distributions that characterize estimation precision and reveal when LaRT achieves smaller asymptotic variances than standalone IRT.

4.1 Identifiability

We next present rigorous identifiability result for the population parameters in LaRT. We begin by defining identifiability for LaRT.

Definition 1. The LaRT model is identifiable at $\boldsymbol{\Omega}$ if, for any other set of parameters $\boldsymbol{\Omega}'$ that gives rise to the same marginal distribution of the observed data, i.e., $P(\mathbf{R}, \mathbf{T}; \boldsymbol{\Omega}) = P(\mathbf{R}, \mathbf{T}; \boldsymbol{\Omega}')$, then $\boldsymbol{\Omega} = \boldsymbol{\Omega}'$ must hold.

The probit link for modeling the response accuracy in LaRT enables rigorous identifiability analyses and guarantees for LaRT. For single-modal IRT model with a probit link, Fang et al. (2021) build their identifiability analysis on a key proposition showing that establishing identifiability reduces to verifying whether the probit thresholds and tetrachoric correlations admit a unique parameterization. While their results do not directly apply to LaRT's hierarchical bimodal structure, they inspire our approach. In particular, we derive an identifiability guarantee for LaRT by following a similar reduction strategy. We first establish Proposition 1, which reduces the identifiability analysis to checking a set of more tractable conditions.

Proposition 1. *Two sets of parameters $(\mathbf{a}, \mathbf{b}, \boldsymbol{\omega}, \boldsymbol{\varphi}, \boldsymbol{\lambda}, \rho)$ and $(\mathbf{a}', \mathbf{b}', \boldsymbol{\omega}', \boldsymbol{\varphi}', \boldsymbol{\lambda}', \rho')$ give rise to the same marginal distribution if and only if*

$$\frac{b_j}{\sqrt{a_j^2 + 1}} = \frac{b'_j}{\sqrt{a_j'^2 + 1}}, \quad \omega_j = \omega'_j, \quad \varphi_j^2 + \lambda_j = \varphi_j'^2 + \lambda'_j,$$

for all $j \in [J]$,

$$\frac{a_{j_1} a_{j_2}}{\sqrt{a_{j_1}^2 + 1} \sqrt{a_{j_2}^2 + 1}} = \frac{a'_{j_1} a'_{j_2}}{\sqrt{a'^2_{j_1} + 1} \sqrt{a'^2_{j_2} + 1}}, \quad \varphi_{j_1} \varphi_{j_2} = \varphi'_{j_1} \varphi'_{j_2},$$

for all $j_1 \neq j_2$,

$$\frac{\rho a_{j_1} \varphi_{j_2}}{\sqrt{a_{j_1}^2 + 1}} = \frac{\rho' a'_{j_1} \varphi'_{j_2}}{\sqrt{a'^2_{j_1} + 1}},$$

for all $j_1, j_2 \in [J]$.

For the parameters associated with response accuracy \mathbf{R} , this proposition requires that the probit thresholds and tetrachoric correlations implied by the marginal distribution of \mathbf{R} admit a unique parameterization. For the parameters associated with CoT \mathbf{T} , it further requires a unique parameterization of the mean and variance of its marginal distribution. In addition, it imposes that the covariance between R_{i,j_1} and T_{i,j_2} remains the same for all $j_1, j_2 \in [J]$. The proof of Proposition 1 is provided in Appendix B.1.

Importantly, checking identifiability of LaRT via the equalities in Proposition 1 parallels the proof strategy used for linear factor models. Let $\tilde{\mathbf{A}}$ denote the discrimination matrix (factor loadings) and $\tilde{\mathbf{\Sigma}}$ the covariance matrix of the latent variables. In that setting, identifiability reduces to verifying the equality $\tilde{\mathbf{A}}\tilde{\mathbf{A}}^\top + \tilde{\mathbf{\Sigma}} = \tilde{\mathbf{A}}'\tilde{\mathbf{A}}'^\top + \tilde{\mathbf{\Sigma}}'$. Anderson et al. (1956) show the identifiability of linear factor models holds under mild conditions. Building on this analogy and the foundational results of Anderson et al. (1956), we establish identifiability for LaRT in Theorem 1.

Theorem 1. *If (1) there are at least 2 non-zero entries in both \mathbf{a} and $\boldsymbol{\varphi}$, (2) $\sum_{j=1}^J a_j > 0$, $\sum_{j=1}^J \varphi_j > 0$, then LaRT is identifiable.*

Condition 1 is standard in the identifiability analysis of generalized linear factor models. For a general K -dimensional setting with factor loading matrix $\tilde{\mathbf{A}} = [\mathbf{a}_1, \dots, \mathbf{a}_J]^\top \in \mathbb{R}^{J \times K}$, it requires that, after deleting any row of $\tilde{\mathbf{A}}$, the remaining matrix still has rank K . In our evaluation context, this condition implies that there must be at least two items that differentiate the latent ability and at least two items that differentiate the latent speed of the LLMs, which is a very mild requirement.

Condition 1 ensures LaRT identifiability only up to a sign indeterminacy arising from the bilinear terms $a_j \theta_i$ and $\varphi_j \tau_i$. To resolve this, we impose the additional constraints $\sum_j a_j > 0$ and $\sum_j \varphi_j > 0$. These constraints enforce interpretable parameter orientations: a higher latent ability corresponds to a higher overall probability of correct responses, and a higher latent speed corresponds to faster responses. In addition, requiring only the sums of a_j and φ_j to be positive is a weaker restriction than the common psychometric assumption that all item discriminations are strictly positive (Hambleton and Swaminathan, 2013). The proof of Theorem 1 is in Appendix B.2.

4.2 Asymptotic Posterior Normality

We now establish the asymptotic normality of the individual latent-variable estimators (θ_i, τ_i) . The asymptotic variances can provide guidance on the estimation precision of the latent-variable estimates as the number of items increases, which is particularly valuable in high-stakes large-scale evaluations such as LLM evaluation, where ranking outcomes can influence user adoption and system deployment decisions. Moreover, as shown later in this section, they offer insight into when LaRT can outperform a standalone IRT model by achieving smaller asymptotic variances.

For general IRT models, Chang and Stout (1993); Kornely and Kateri (2022) present results on the asymptotic distribution of latent ability. In what follows, we derive the asymptotic distribution of the latent variables (θ_i, τ_i) in LaRT, with additional considerations arising from the CoT

component of the model. Since (θ_i, τ_i) are independent across LLMs conditional on the population parameters, we drop the subscript i and use the generic notation $\boldsymbol{\xi} = (\theta, \tau)$. We require three regularity conditions on the response-time component for establishing the asymptotic distribution, following [Chang and Stout \(1993\)](#); [Kornely and Kateri \(2022\)](#). We defer the specific forms of the three mild regularity assumptions and discussions to [Appendix C.1](#). We establish the asymptotic distribution of the latent traits in [Theorem 2](#).

Theorem 2. *Let $\mathbf{z} \sim N_2(0, \mathbf{I}_2)$, $\{R_j, T_j\}_{j \in \mathbb{N}} \sim \mathcal{P}(\boldsymbol{\xi}_0)$, $\boldsymbol{\xi}_0 \in \Theta \setminus \partial\Theta$. Under [Assumption 1, 2, 3](#), for all $B \in \mathcal{B}(\Theta)$, for a fixed $\boldsymbol{\xi}_0$,*

$$P\left(\tilde{\mathcal{I}}_J(\tilde{\boldsymbol{\xi}}_J)^{1/2}(\boldsymbol{\xi} - \tilde{\boldsymbol{\xi}}_J) \in B \mid \mathbf{R}^{(J)}, \mathbf{T}^{(J)}\right) \xrightarrow{P_{\boldsymbol{\xi}_0}} P(\mathbf{z} \in B), \quad J \rightarrow \infty.$$

If $\boldsymbol{\xi}_0 \sim \mathcal{G}$, where \mathcal{G} is an absolutely continuous proper distribution whose support is within Θ ,

$$P\left(\tilde{\mathcal{I}}_J(\tilde{\boldsymbol{\xi}}_J)^{1/2}(\boldsymbol{\xi} - \tilde{\boldsymbol{\xi}}_J) \in B \mid \mathbf{R}^{(J)}, \mathbf{T}^{(J)}\right) \xrightarrow{P} P(\mathbf{z} \in B), \quad J \rightarrow \infty.$$

The proof of [Theorem 2](#) is in [Appendix C.1](#). To further analyze the factors contributing to the variance of θ , we present the explicit expression for its inverse variance, i.e., the precision $\tilde{\mathcal{I}}_J(\theta)$, as follows:

$$\tilde{\mathcal{I}}_J(\theta) = \frac{1}{1 - \rho^2} + \sum_{j=1}^J \frac{a_j^2 \phi(a_j \theta_i + b_j)^2}{\Phi(a_j \theta_i + b_j)[1 - \Phi(a_j \theta_i + b_j)]}. \quad (10)$$

Here, the second term corresponds to the Fisher information, while the first term depends on the correlation between the latent ability and latent speed. In particular, $\tilde{\mathcal{I}}_J(\theta)$ increases as $|\rho|$ increases, implying that the variance decreases as $|\rho|$ increase and is maximized at $\rho = 0$, which corresponds to the IRT case where CoT information is ignored. Consequently, the asymptotic estimation precision of θ under LaRT exceeds that of IRT whenever the latent ability and latent speed are correlated.

5 Simulation Study

We conduct a simulation study that emulates the characteristics of the real-world application. These simulations serve two primary objectives. First, we validate the performance of our proposed SAEM algorithm with the data-driven initialization and the MAP estimate of latent traits. Second, we demonstrate the superiority of LaRT over standard IRT in terms of finite-sample estimation accuracy of the latent ability. For the IRT baseline, we estimate the population parameters \mathbf{a} and \mathbf{b} using the SAEM approach described by [Li et al. \(2025\)](#), and estimate the latent ability $\boldsymbol{\theta}$ using the similar MAP method detailed in [Section 3.3](#). Unless otherwise noted, all subsequent implementations of IRT follow this procedure.

The simulation design is as follows. Each entry of \mathbf{a} is drawn from $\text{Unif}(0.5, 1)$, \mathbf{b} from $N(0, 0.5)$, $\boldsymbol{\omega}$ from $N(0, 1)$, $\boldsymbol{\varphi}$ from $\text{Unif}(0.5, 1.5)$, $\boldsymbol{\lambda}$ from $\text{Unif}(0.5, 2)$. We set $\rho = -0.8$. We fix $J = 50$, and let $N \in \{100, 200, 500\}$. For each simulation setting, we perform 200 independent replications.

The simulation results are presented in [Figure 1](#) and [2](#). [Figure 1](#) shows that LaRT achieves better estimation accuracy than IRT for all $\boldsymbol{\theta}$, \mathbf{a} , and \mathbf{b} . For other parameters $\boldsymbol{\varphi}$, $\boldsymbol{\omega}$, $\boldsymbol{\lambda}$, and ρ , the simulation results confirm that as N increases, the estimation error decreases.

Comparison between LaRT and IRT when $\rho = -0.8$

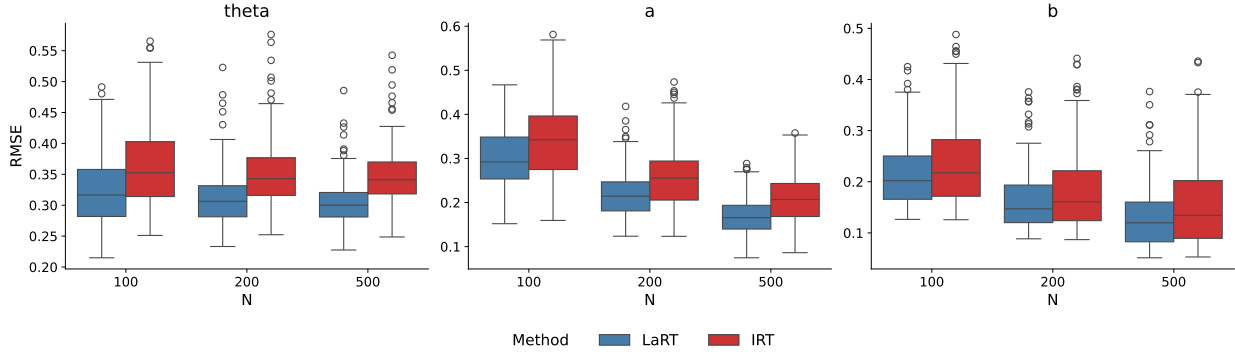


Figure 1: RMSEs of IRT and LaRT when $\rho = -0.8$. LaRT performs uniformly better than IRT. As N grows, RMSE of \hat{a} and \hat{b} decreases when J is fixed.

Estimation Accuracy of LaRT when $\rho = -0.8$

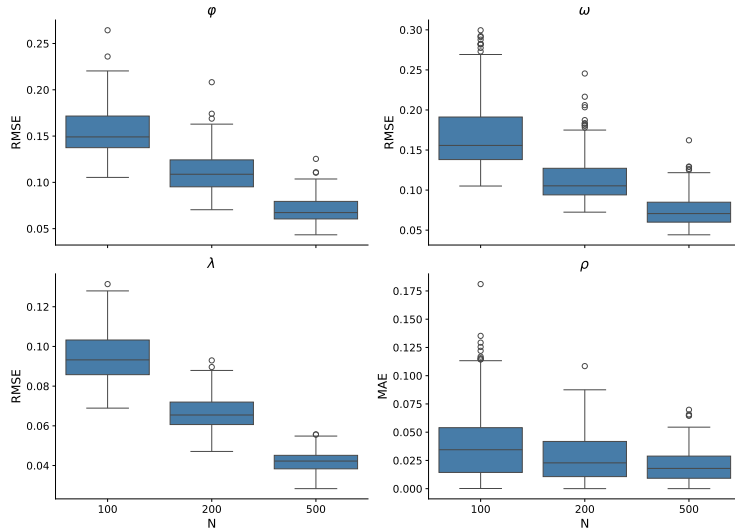


Figure 2: Boxplot of estimation accuracy of other parameters of LaRT when $\rho = -0.8$ in RMSE and MAE. The metric is presented in the plot. As N grows, the estimation error of all parameters decreases.

6 Applications to Real LLM Data

We evaluated over 80 open-source LLMs on four math reasoning benchmark datasets: MATH500 (Hendrycks et al., 2021), AMC23, AIME24, and AIME25, containing 500, 40, 30, and 30 questions respectively. These benchmarks consist of advanced high school competition problems ordered by increasing difficulty, with MATH500 being the easiest and AIME25 being the hardest. The evaluated LLMs range in parameter size from 0.6 billion to 32 billion; a complete list is provided in Appendix E. Following prior work Castleman et al. (2025), we respectively evaluate these LLMs with zero-shot and one-shot chain-of-thought prompts to increase the number of evaluated LLMs (see Appendix E for prompt details).

When collecting response data from LLMs, we set the maximum CoT length to 10,240 tokens. This limit is generous for mathematical reasoning, as ground truth solutions in the MATH dataset rarely exceed 1,000 tokens (Hendrycks et al., 2021). By setting the limit to 10,240, we allow LLMs to utilize ten times the token budget of human references. Furthermore, this setting aligns with the “medium-to-high” reasoning regime defined by Agarwal et al. (2025), who evaluated gpt-oss across limits of 1,000, 6,000, and 16,000 tokens. Detailed hyperparameter configurations are in Appendix E.

After obtaining LLMs’ responses to each math problem, we use each LLM’s tokenizer to count the length of their CoT. We delete LLMs who failed to answer any question correctly in these four benchmarks. After data preprocessing, there are 138 LLMs for further evaluation.

Given this collected dataset of LLM responses, we apply LaRT to evaluate LLMs on these representative math benchmarks. First, we visualize the evaluation results based on the estimated latent ability and latent speed to assess consistency and demonstrate how LaRT automatically adjusts rankings by accounting for item characteristics across benchmarks. A key finding is strong negative correlation between ability and speed: higher-ability LLMs produce longer CoT. Second, we examine the benchmark characteristics through the estimated population parameters, highlighting their difficulty levels and discriminative power. We also compare LaRT and IRT across four key evaluation metrics from the LLM evaluation literature (Subsection 6.2) and quantitatively demonstrate LaRT’s superiority over IRT across all four (Subsection 6.3).

In this section, we present a comprehensive analysis that jointly examines LLM performance, benchmark characteristics, and the effectiveness of LaRT across the math datasets introduced above. First, we visualize evaluation outcomes based on estimated latent ability and latent speed across benchmarks, providing insights into LLM ranking, and the relationship between latent ability and latent speed. Second, leveraging the estimated population parameters, we investigate general trends in item characteristics within and across benchmarks, and illustrate how LaRT improves discriminative utility beyond accuracy-based evaluation. Third, we compare the LLM rankings produced by IRT and LaRT: we not only illustrate representative ranking shifts and explain their causes, but also conduct comprehensive quantitative experiments to demonstrate that LaRT offers more convincing evaluation results with respect to the desiderata of predictive power, item efficiency, validity, and LLM efficiency.

6.1 Qualitative Evaluation

First, we present the scatter plots of estimated latent speed against latent ability, as well as the estimated correlation ρ between the latent ability and latent speed in Figure 3. Across all datasets, ρ is strongly negative, confirming that LLMs with stronger math reasoning ability have longer CoT, a highly intuitive result. Moreover, the absolute value of ρ increases as the questions in the dataset becomes more difficult, indicating that harder questions require more test-time compute. As $|\rho|$ gets larger, the CoT modeling contributes more to the estimation of the latent ability for each LLM. Thus, this phenomenon implies LaRT may offer greater advantages on more challenging benchmarks.

For the estimated population parameters, we present the boxplots of estimated parameters for accuracy and latency respectively in Figure 4 and 5. Specifically, we transform \mathbf{b} into $\tilde{\mathbf{b}} = -\mathbf{b}/\mathbf{a}$. In this way, the probability of LLM i answering item j correctly is $\Phi(a_j(\theta_i - \tilde{b}_j))$, and \tilde{b}_j can be interpreted as the difficulty level of item j . Similarly, we transform $\boldsymbol{\omega}$ into $\tilde{\boldsymbol{\omega}} = \boldsymbol{\omega}/\boldsymbol{\varphi}$. Since there are items whose discrimination \mathbf{a} is close to 0 or negative, we delete all entries whose discrimination a_j is less than 0.05 to better present the boxplot of $\tilde{\mathbf{b}}$.

For \mathbf{a} and \mathbf{b} , as the benchmark dataset becomes more difficult, the estimated difficulty param-

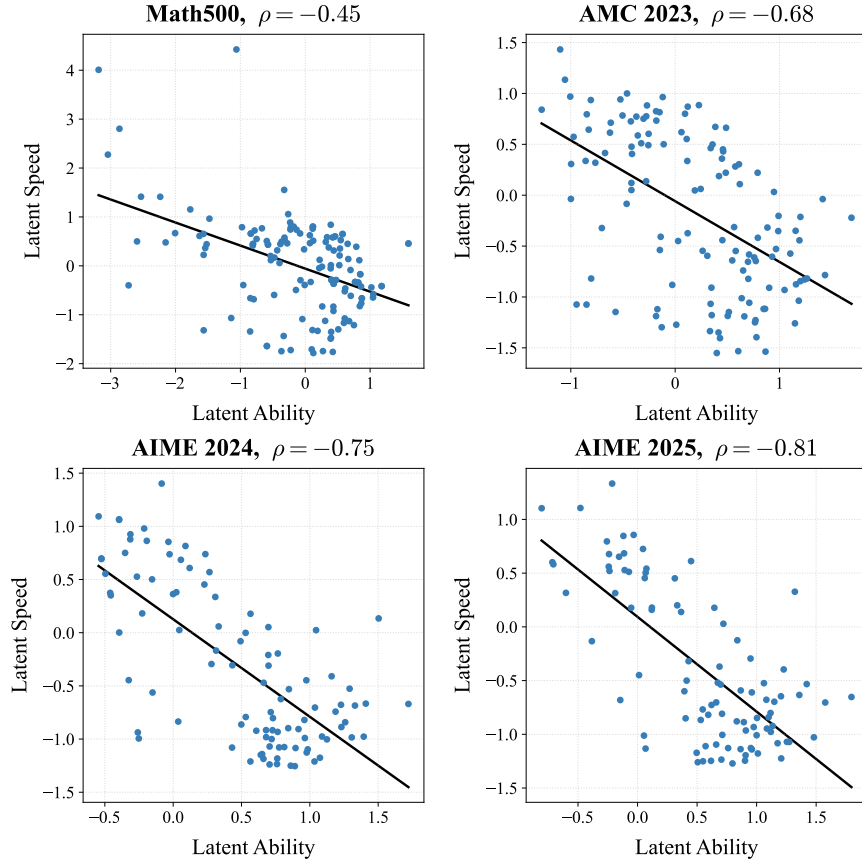


Figure 3: Scatter plot of estimated latent speed against latent ability for each dataset. The estimated correlation for each dataset is presented in the subtitle. LLMs with stronger latent ability has a smaller latent speed (longer CoT length). As the dataset becomes more difficult, the estimated correlation ρ increases in absolute value.

ters increase monotonically. Given its relatively large size, MATH500 captures a broad spectrum of difficulty, including some highly challenging items. This shows the validity of estimated population parameters by LaRT. For the discriminative parameters \mathbf{a} , as the dataset becomes more difficult, the discriminative power increases, except AIME25. Since we are testing relatively small LLMs, AIME25 can be too difficult for most of the tested LLMs. Thus, in general, items in AIME25 have less discriminative power in comparison with the easier datasets. Additionally, there are a small proportion of items in these 4 datasets that have close to 0 or negative discriminative power. This is a common phenomenon in LLM benchmarking datasets. This can result from the wrong answers of question items, or the wrong grading (Gema et al., 2025). Through learning the discriminative parameters of question items, LaRT can automatically adjust for this issue. Furthermore, from Theorem 1, the estimated parameters satisfy the identifiability conditions. Our mild identifiability conditions do not require that every item should have a positive discriminative parameter, which adapts well to the misgrading issue in LLM ranking.

For φ , $\tilde{\omega}$, and $\boldsymbol{\lambda}$, all the estimated parameters are strictly positive. The identifiability conditions in Theorem 1 are satisfied. For the basic latency level, as the difficulty of the dataset increases, the base CoT length increases, except for AIME25. This may result from the same issue as explained in the previous paragraph about the discriminative parameters. Since AIME25 is too difficult for

most of the tested LLMs, some LLMs fail to provide a valid CoT, and indeed answers the question incorrectly with a shorter CoT length. For the discriminative parameter of latency, there is no significant trend as the benchmark dataset becomes more difficult. As one can see in Figure 12, some best performing LLMs are able to use shorter test-time computing to solve simpler problems. For example, as the difficulty of the dataset increases, the latent speed of Qwen3-30B-A3B-Instruct-2507 decreases sharply. We will discuss possible directions for a more refined model for CoT length in the discussion section.

Figure 6 presents the scatterplot of estimated discrimination of response accuracy a against the discrimination of latent speed φ . We only present the question items whose discriminative power is less than 0.5. Several items exhibit minimal discriminative power for latent ability yet possess significant discriminative power for latent speed. Conceptually, extremely easy or difficult items yield uniform response accuracy, resulting in a small value of a , because few LLMs answer them correctly/wrong. However, joint modeling of accuracy and CoT length allows us to additionally evaluate CoT quality on these items. Consequently, the overall discriminative utility of questions with low discriminative power in accuracy is enhanced.

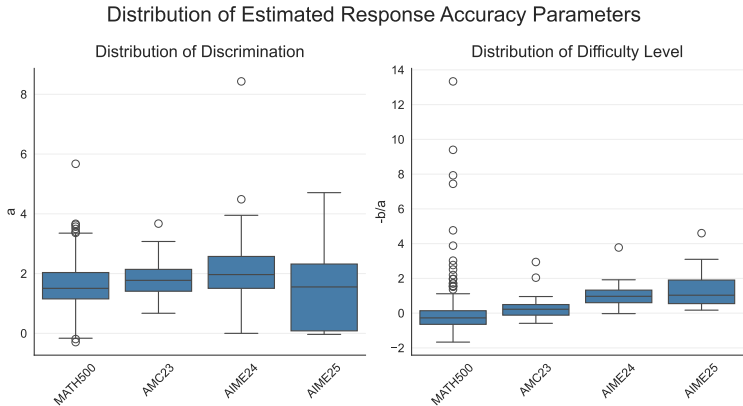


Figure 4: Boxplots of a and b for 4 datasets estimated by LaRT. The plot on the left is the boxplot of a . The plot on the right is the boxplot of $-b/a$. Except the most difficult AIME25, as the dataset becomes more difficult, the average discriminative power of accuracy increases.

Additionally, we present the asymptotic confidence intervals estimated by Theorem 2 in MATH500 for zero-shot models in Figure 7. The LLMs are ordered by their estimated θ . With the confidence interval estimate, we can conclude whether an LLM outperforms the other LLM with statistical significance. Since $\sqrt{sd_1^2 + sd_2^2} \leq sd_1 + sd_2$, if the upper limit of the confidence interval of LLM A is smaller than the lower limit of the confidence interval of LLM B, then with rejection level of at least 0.05, we can conclude LLM B has better latent ability in this dataset than LLM A. For example, we can conclude with 95% confidence that Qwen3-30B-A3B-Instruct-2507 is better than Nvidia-Acereason-Nemotron-1.1-7B.

To give a direct comparison between the rankings given by IRT and LaRT, Figure 8 presents LLMs whose rankings given by these two models differ. Ranking differences for other IRT datasets are presented in Appendix F. Figure 8 shows that many LLMs’ rankings differ between IRT and LaRT. The difference results from LLMs that correctly answer similar numbers of items, but differs in CoT length. In general, LLMs with longer CoT length has higher ranking by LaRT compared with IRT.

Specifically, we look at the shift in rankings in Qwen3-30B-A3B-Thinking-2507 (shorthand as Qwen-Thinking), Qwen3-30B-A3B-Instruct-2507 (shorthand as Qwen-Instruct), and Qwen3-32B in

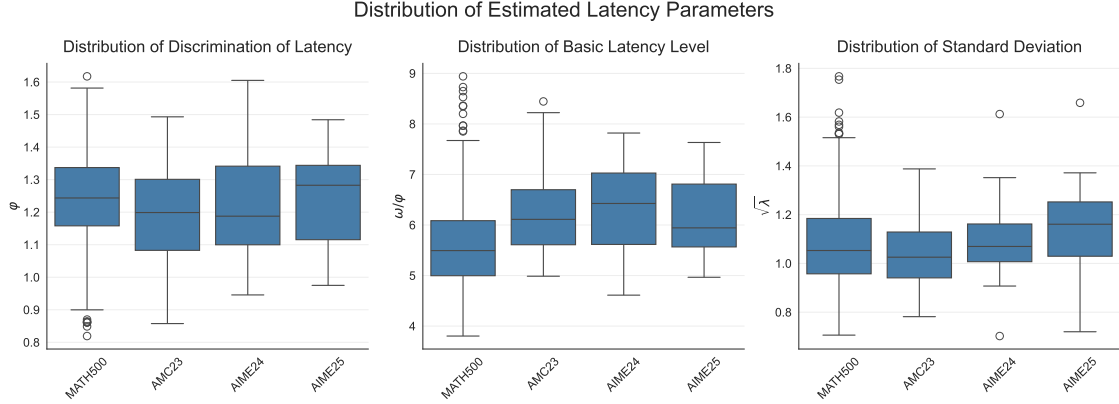


Figure 5: Boxplots of φ , ω , and λ for 4 datasets estimated by LaRT. The left plot is the distribution of φ . The middle plot is the boxplot of ω/φ . The right plot is the boxplot of λ . Except AIME25, as the dataset becomes more difficult, the basic latency level increases.

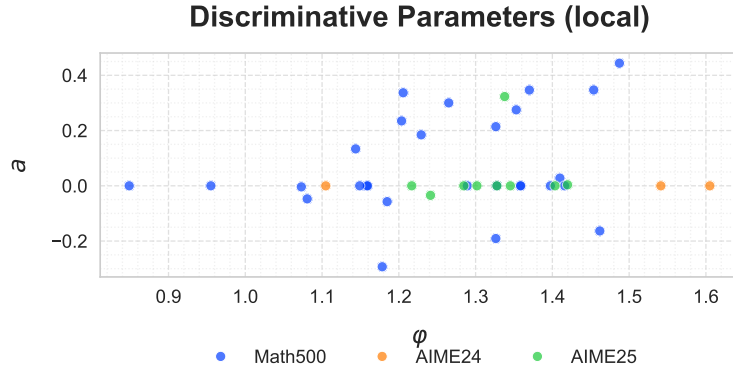


Figure 6: Scatterplot of estimated discrimination of the latent ability a against the discrimination of latent speed φ for questions with small discriminative ability for the latent ability a . The color of the points represent different datasets as shown in the legend. There are many questions with minimal discriminative power in accuracy, but significant positive discriminative power in CoT length.

the zero-shot prompting. Qwen-Thinking, Qwen-Instruct, and Qwen3-32B correctly answer 15, 14, and 14 questions respectively, and have average CoT length of 5168, 5922, and 8333 respectively. In the ranking by IRT, Qwen-Thinking is better than Qwen-Instruct, and Qwen-Instruct is better than Qwen3-32B. In the ranking by LaRT, Qwen-Instruct is better than Qwen-Thinking, and Qwen-Thinking is better than Qwen3-32B. The larger test-time compute for Qwen-Instruct helps it surpass Qwen-Thinking in the ranking by LaRT. However, even though the CoT length for Qwen3-32B is significantly larger than both Qwen-Instruct and Qwen-Thinking, the ranking of Qwen3-32B remains the same. Especially, Qwen3-32B answers the same number of items correctly as Qwen-Instruct. This illustrates how LaRT’s probabilistic modeling automatically balances difficulty, time requirements, and discrimination in both accuracy and latency. We demonstrate quantitatively that LaRT produces more convincing rankings in the next subsection.

LaRT on Math500 for Zero-Shot Models with 95% Confidence Interval

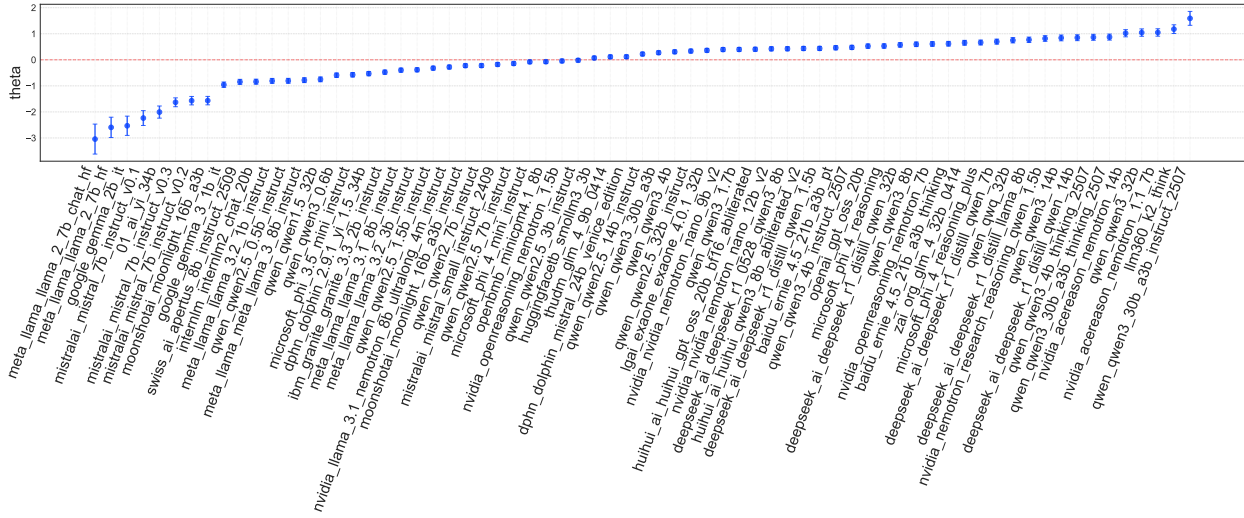


Figure 7: Latent ability estimates for zero-shot models on the MATH500 dataset using LaRT. The error bars represent 95% asymptotic confidence intervals. Non-overlapping intervals indicate statistically significant differences in performance between LLMs.

Comparison of Model Rankings for AIME25

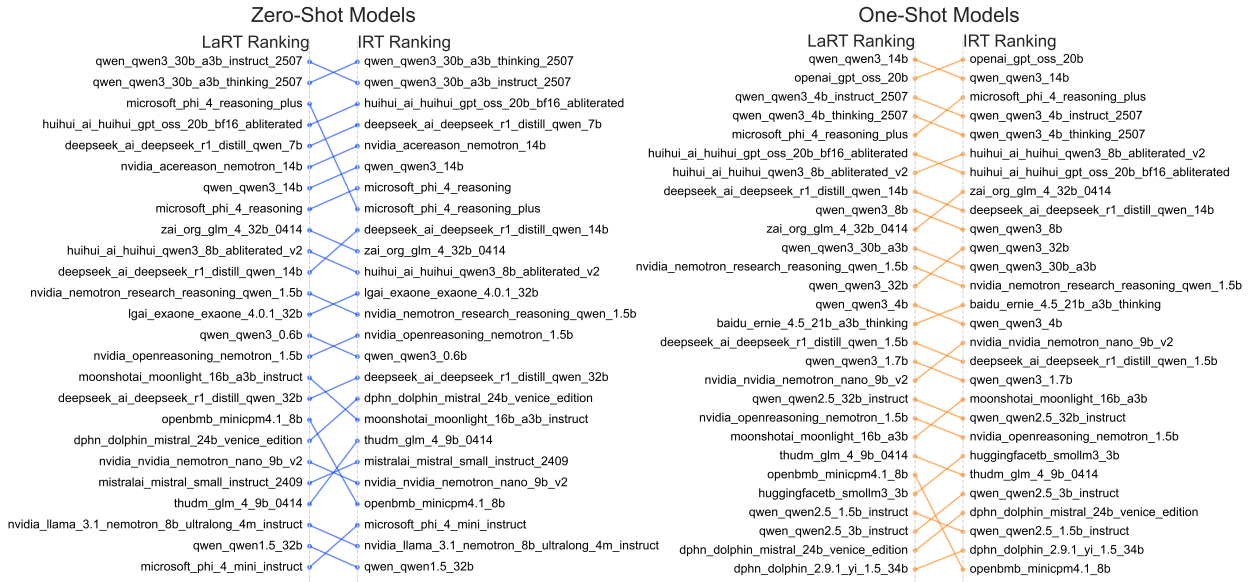


Figure 8: Differences in LLM rankings for both zero-shot models and one-shot models for AIME25. The left figure is for zero-shot models, and the right figure for one-shot models. For each of the figure, rankings by LaRT are on the left, and rankings by IRT on the right. LLMs that are higher have higher ranking. The lines connect the same models with different rankings by LaRT and IRT.

6.2 Desiderata for LLM Evaluation Benchmark

This section introduces four desiderata for evaluating LLM benchmarking methods, motivated by prior work (Maia Polo et al., 2024; Hofmann et al., 2025), covering both active and static

evaluation settings. The first two desiderata address active evaluation, while the final two address static evaluation. We use these four dimensions to compare the performance of LaRT against IRT.

1. **Predictive Power** refers to the ability to accurately predict LLM performance on unseen items using a limited set of questions (Maia Polo et al., 2024). A method with higher predictive power extracts more information from the response data. Held-out predictive power is a standard measure of model fit in statistics (Gelman et al., 1996).
2. **Item Efficiency**: Measures the number of items required to accurately estimate an LLM’s latent ability. IRT with CAT has shown better efficiency in LLM ranking than other methods (Zhuang et al., 2023; Hofmann et al., 2025).
3. **Validity**: Measures the consistency of LLM rankings across different datasets. High consistency is a desirable trait of a robust benchmarking method. IRT-based methods have previously shown strong performance in this area (Hofmann et al., 2025).
4. **LLM Efficiency**: Measures the number of LLMs required to accurately estimate population parameters for active evaluation. Reducing this number is vital, as full evaluations are resource-intensive, potentially costing thousands of GPU hours for each LLM (Liang et al., 2023).

Previous literature focused on ranking consistency (Hofmann et al., 2025). However, in our comparison of IRT and LaRT, we focus on latent ability estimation as a reliable metric. Figure 12 shows that minor perturbations in ability estimates can cause drastic changes in an LLM’s final rank. We therefore compare latent ability estimation accuracy rather than ranking outcomes, as ability estimates are more robust to perturbations.

6.3 Quantitative Comparison

6.3.1 Predictive Power

We test the predictive power of LaRT in comparison with IRT under the active evaluation setting. Prior works on predictive accuracy also studied the active evaluation regime (Maia Polo et al., 2024). We concatenate AMC23, AIME24, and AIME25 datasets together. We delete LLMs that fail to answer any of the questions correctly. After preprocessing, there are $N = 128$ LLMs and $J = 100$ question items. We randomly select $N_t = 100$ LLMs as training set to estimate the population parameters in LaRT. For the test set, we examine the prediction performance via five-fold cross-validation. We randomly partition the $J = 100$ questions into five disjoint sets. For each fold, we first obtain the LLMs’ latent abilities with four sets of questions. Then, we predict the responses of each LLM for the questions in the remaining test set. Since both the correct/wrong responses and predicted probability of each item are within $[0, 1]$, we use mean absolute error as the metric for the prediction accuracy.

The result for each fold and average mean absolute error is presented in Table 1. LaRT significantly outperforms IRT in all folds. This illustrates that LaRT is able to extract more information from the data in comparison with IRT.

6.3.2 Item Efficiency

For item efficiency, we measure how many questions are needed to estimate the latent ability of each LLM accurately. We take on the computerized adaptive testing (CAT, Meijer and Nering,

Fold	1	2	3	4	5	Average
LaRT	0.235	0.177	0.183	0.160	0.161	0.183
IRT	0.391	0.190	0.268	0.257	0.238	0.269

Table 1: Prediction Accuracy of LaRT and IRT in Mean Absolute Error. LaRT uniformly predicts responses in unseen entries more accurately than IRT.

1999; Wainer et al., 2000; Chang, 2015) perspective to determine which question to add at each time. CAT has gained great popularity in LLM evaluation with IRT (Zhuang et al., 2023; Hofmann et al., 2025). Specifically, we first give every LLM the first 10 questions. According to their answers, we can estimate their latent abilities. For the estimated latent ability of each LLM, we choose an item that maximizes the Fisher information among the rest of the question items. Statistically, by choosing questions that maximize the Fisher information, we can adaptively obtain the least variance in estimating the latent ability (Reckase, 2006). For LaRT, at each time, we choose the item that maximizes the Fisher information for θ_i , whose form is presented in (10).

In the experiment, similarly as Section 6.3.1, we concatenate AMC23, AIME24, and AIME25 together, and delete LLMs that fail to answer any of the questions correctly. We assume the ground truth of the latent ability θ is the $\hat{\theta}$ estimated with all the items in the concatenated dataset. Let $\hat{\theta}_j$ be the estimated latent ability with j question items for each LLM. Note that for each LLM, the j -th question items can be different. We compare the scaled Euclidean distance between $\hat{\theta}_j$ and $\hat{\theta}_J$ for each j . We plot how the scaled Euclidean distance evolve as the number of questions increase in Figure 9.

Figure 9 shows that, in most questions, LaRT estimates the latent ability more accurately than IRT. By incorporating the CoT information, LaRT essentially has more data to estimate the latent ability. Therefore, even with a limited number of items, LaRT is able to estimate the latent ability more accurately.

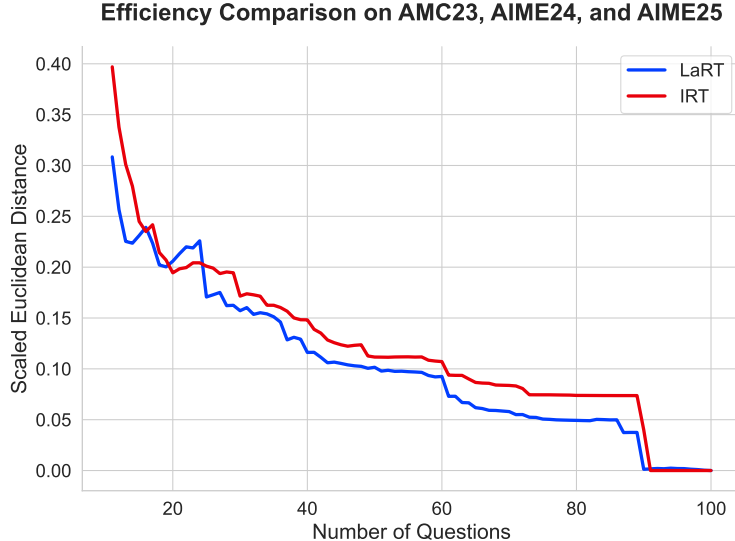


Figure 9: Comparison of Item Efficiency between LaRT and IRT. LaRT can estimate the latent abilities of LLMs accurately with less question items than IRT.

6.3.3 Validity

Prior works have shown IRT-based methods have significant advantage in validity compared with other ranking methods (Hofmann et al., 2025). Therefore, if we observe that LaRT outperforms IRT, then it is reasonable to conclude that LaRT enjoys better validity over other ranking methods.

In this experiment, we randomly partition the questions in MATH500 into 5 non-overlapping sets, where each set contains 100 questions. We apply both LaRT and IRT to each set of questions, and estimate the latent ability of each LLM. We calculate the variance of the estimated latent ability for every LLM, and take the sum of the variances over the 138 LLMs.

The variance of the latent ability estimated by LaRT over five non-overlapping sets is 2.0130, compared to 2.3423 for IRT. LaRT significantly reduces the variance of the estimated latent ability across all subsets of MATH500. Figure 3 show that, MATH500 exhibits the smallest $|\rho|$, which suggests that CoT modeling provides the least assistance for the latent ability estimation compared to other benchmark datasets. LaRT’s ability to significantly decrease variance even for the MATH500 dataset suggests that LaRT may offer greater validity improvements over IRT when applied to more challenging benchmark datasets.

6.3.4 LLM Efficiency

For LaRT estimation efficiency, we evaluate how many LLMs are needed to yield a good estimate of the population parameters. The accuracy of population parameters is crucial to the active evaluation. First, it determines how well we can estimate the latent ability, since the population parameters are fixed when performing MAP estimation for the individual latent variables. Second, we select the question to assign to each LLM adaptively based on the Fisher information. If the population parameters are poorly estimated, the efficacy of this adaptive procedure will be hampered.

In this specific experiment, we select 100 question items in MATH500 with the largest Fisher information averaged over all LLMs. We randomly permute the 140 LLMs and train LaRT and IRT using cumulative subsets of size $N \in \{50, 75, 100, 125, 140\}$. These subsets are nested, such that the set of LLMs used for a smaller sample size is strictly contained within the set for any larger sample size. We treat $\hat{\mathbf{a}}$ and $\hat{\mathbf{b}}$ estimated with the full 140 LLMs as the ground truth. We evaluated convergence by the scaled Euclidean distance between the estimates $\hat{\mathbf{a}}_N, \hat{\mathbf{b}}_N$ at each N , and the ground truth. The result is presented in Table 2.

Table 2 shows that LaRT outperforms IRT in most of the different N . Specifically, the drastic improvement when $N = 50$ is particularly striking. When N is small, two possible scenarios may happen that result in a bad estimate of \mathbf{a} or \mathbf{b} . For \mathbf{b} , suppose there is item j that almost every LLM answers correctly (or almost every LLM answers incorrectly), and hence \hat{b}_j is close to ∞ (or $-\infty$). For \mathbf{a} , suppose there is item j that all LLMs with $\theta_i > 0$ answer it correctly, and all LLMs with $\theta_i < 0$ answer it wrong. Then, \hat{a}_j will be ∞ . Due to these two major difficulties for IRT, when $N = 50$, IRT has unusable estimates of \mathbf{a} and \mathbf{b} , while LaRT leverages CoT length for valid estimation.

N	50		75		100		125	
Method	IRT	LaRT	IRT	LaRT	IRT	LaRT	IRT	LaRT
\mathbf{a}	28.8248	3.8537	5.5137	5.6749	0.9078	0.8896	0.6288	0.5825
\mathbf{b}	18.5782	2.3181	2.7583	3.0197	0.7409	0.7105	0.7464	0.7010

Table 2: Comparison between IRT and LaRT in LLM efficiency. LaRT can estimate the population parameters more accurately with fewer LLMs.

7 Discussion

We proposed the **Latency-Response Theory** model (LaRT) for LLM evaluation in both static and active evaluation settings, with efficient SAEM estimation using spectral initialization. We justify our modeling choice via rigorous theoretical results in both identifiability and asymptotic distribution. In simulation studies, we confirm LaRT achieves better estimation accuracy and confidence interval coverage. In real-data application, we generate the responses and chain-of-thought (CoT) of LLMs in multiple popular datasets ourselves. Through comprehensive comparison in *Predictive Power, Item Efficiency, Validity, LLM Efficiency*, we find that LaRT has outstanding performance in all four dimensions.

This work opens up multiple directions for future research. First, LaRT may improve saturation resistance, which is a major concern for LLM evaluation (Liang et al., 2023). Due to the rapid development of LLMs, the most advanced models can solve most items in the benchmark dataset. If two LLMs solve exactly the same items correctly, IRT is unable to distinguish their latent ability. However, thanks to the additional information from the CoT length, LaRT is able to provide a more refined latent ability estimation, distinguishing LLMs even if they answer the same items correctly. While we only considered open-source small-to-medium size LLMs for evaluation, it will be a fruitful direction to explore LaRT’s performance in saturated dataset in the future.

Second, our algorithmic and theoretical results for LaRT extend naturally to multidimensional latent abilities. If the goal of LLM evaluation is to predict the response for future question items, extending \mathbf{a} , $\boldsymbol{\theta}$, $\boldsymbol{\varphi}$, $\boldsymbol{\tau}$ from one dimension to multiple dimensions can help extract more information from the data. Maia Polo et al. (2024) applies Multidimensional Item Response Theory models to predict the responses of future question items. Based on the real data application, we believe extending LaRT to multiple dimensions will achieve even better predictive performance.

Third, LaRT’s flexibility allows incorporating other covariates that are highly correlated with latent ability. For example, the CoT reasoning themselves contain rich information about an LLM’s reasoning ability. Integrating this data directly into the LaRT framework could substantially enhance ranking performance. Prior work has used LLM graders to evaluate step-by-step CoT reasoning, essentially yielding binary tensor data (Xia et al., 2025). The step-by-step grading can serve as another summary of the information contained in the CoT. The LaRT framework can model these binary correct/wrong outcomes, using a probit link, to further refine the estimation of LLM latent abilities. Other considerations such as environmental impact (Liang et al., 2023) can also be summarized as an additional covariate to modify the rankings of LLMs.

By jointly modeling response accuracy and CoT length, LaRT significantly advances key evaluation desiderata. Nevertheless, deviations from this general trend exist. For instance, on challenging items, certain LLMs may engage in extended but erroneous reasoning processes, yielding long CoT sequences despite incorrect outcomes. Future work could address this heterogeneity via mixture modeling to disentangle CoT length distributions conditional on response correctness (Wang and Xu, 2015).

Finally, beyond LLM evaluation, this work contributes new methodology with sound theoretical guarantee to the field of psychometrics. Our methods can be readily deployed in educational assessment applications and used to analyze student test takers’ response data.

Supplementary Material. The supplementary material contains proofs of all theoretical results. It also presents additional simulation studies comparing the performance of SAEM with data-driven initialization against the traditional SAEM approach, along with additional results for the real data application.

References

- Agarwal, S., Ahmad, L., Ai, J., Altman, S., Applebaum, A., Arbus, E., Arora, R. K., Bai, Y., Baker, B., Bao, H., et al. (2025). gpt-oss-120b & gpt-oss-20b model card. *arXiv preprint arXiv:2508.10925*.
- Anderson, T. W., Rubin, H., et al. (1956). Statistical inference in factor analysis. In *Proceedings of the third Berkeley symposium on mathematical statistics and probability*, volume 5, pages 111–150.
- Bolsinova, M. and Tijmstra, J. (2019). Modeling differences between response times of correct and incorrect responses. *psychometrika*, 84(4):1018–1046.
- Camilli, G. and Geis, E. (2019). Stochastic approximation em for large-scale exploratory irt factor analysis. *Statistics in medicine*, 38(21):3997–4012.
- Castleman, J., Nadeem, N., Namjoshi, T., and Liu, L. T. (2025). Rethinking math benchmarks for LLMs using IRT. *Proceedings of Machine Learning Research*, 273:66–82.
- Chang, H.-H. (2015). Psychometrics behind computerized adaptive testing. *Psychometrika*, 80(1):1–20.
- Chang, H.-H. and Stout, W. (1993). The asymptotic posterior normality of the latent trait in an irt model. *Psychometrika*, 58(1):37–52.
- Chang, H.-H. and Ying, Z. (1996). A global information approach to computerized adaptive testing. *Applied Psychological Measurement*, 20(3):213–229.
- Chen, M. (2021). Evaluating large language models trained on code. *arXiv preprint arXiv:2107.03374*.
- Cobbe, K., Kosaraju, V., Bavarian, M., Chen, M., Jun, H., Kaiser, L., Plappert, M., Tworek, J., Hilton, J., Nakano, R., et al. (2021). Training verifiers to solve math word problems. *arXiv preprint arXiv:2110.14168*.
- De Boeck, P. and Jeon, M. (2019). An overview of models for response times and processes in cognitive tests. *Frontiers in psychology*, 10:102.
- Delyon, B., Lavielle, M., and Moulines, E. (1999). Convergence of a stochastic approximation version of the em algorithm. *The Annals of Statistics*, 27(1):94–128.
- Durante, D. (2019). Conjugate bayes for probit regression via unified skew-normal distributions. *Biometrika*, 106(4):765–779.
- Ein-Dor, L., Halfon, A., Gera, A., Shnarch, E., Dankin, L., Choshen, L., Danilevsky, M., Aharonov, R., Katz, Y., and Slonim, N. (2020). Active Learning for BERT: An Empirical Study. In Webber, B., Cohn, T., He, Y., and Liu, Y., editors, *Proceedings of the 2020 Conference on Empirical Methods in Natural Language Processing (EMNLP)*, pages 7949–7962, Online. Association for Computational Linguistics.
- Entink, R. K., Fox, J.-P., and van der Linden, W. J. (2009). A multivariate multilevel approach to the modeling of accuracy and speed of test takers. *Psychometrika*, 74(1):21–48.

- Fang, G., Guo, J., Xu, X., Ying, Z., and Zhang, S. (2021). Identifiability of bifactor models. *Statistica Sinica*, 31:2309–2330.
- Fox, J.-P. and Marianti, S. (2016). Joint modeling of ability and differential speed using responses and response times. *Multivariate behavioral research*, 51(4):540–553.
- Gelman, A., Meng, X.-L., and Stern, H. (1996). Posterior predictive assessment of model fitness via realized discrepancies. *Statistica sinica*, pages 733–760.
- Gema, A. P., Leang, J. O. J., Hong, G., Devoto, A., Mancino, A. C. M., Saxena, R., He, X., Zhao, Y., Du, X., Madani, M. R. G., et al. (2025). Are we done with mmlu? In *Proceedings of the 2025 Conference of the Nations of the Americas Chapter of the Association for Computational Linguistics: Human Language Technologies (Volume 1: Long Papers)*, pages 5069–5096.
- Guo, D., Yang, D., Zhang, H., Song, J., Zhang, R., Xu, R., Zhu, Q., Ma, S., Wang, P., Bi, X., et al. (2025). Deepseek-r1: Incentivizing reasoning capability in llms via reinforcement learning. *arXiv preprint arXiv:2501.12948*.
- Hambleton, R. K. and Swaminathan, H. (2013). *Item response theory: Principles and applications*. Springer Science & Business Media.
- Hendrycks, D., Burns, C., Kadavath, S., Arora, A., Basart, S., Tang, E., Song, D., and Steinhardt, J. (2021). Measuring mathematical problem solving with the math dataset. *NeurIPS*.
- Hofmann, V., Heineman, D., Magnusson, I., Lo, K., Dodge, J., Sap, M., Koh, P. W., Wang, C., Hajishirzi, H., and Smith, N. A. (2025). Fluid language model benchmarking. In *Second Conference on Language Modeling*.
- Jaech, A., Kalai, A., Lerer, A., Richardson, A., El-Kishky, A., Low, A., Helyar, A., Madry, A., Beutel, A., Carney, A., et al. (2024). Openai o1 system card. *arXiv preprint arXiv:2412.16720*.
- Kipnis, A., Voudouris, K., Buschhoff, L. M. S., and Schulz, E. (2025). metabench - a sparse benchmark of reasoning and knowledge in large language models. In *The Thirteenth International Conference on Learning Representations*.
- Klein Entink, R. H., Kuhn, J.-T., Hornke, L. F., and Fox, J.-P. (2009). Evaluating cognitive theory: a joint modeling approach using responses and response times. *Psychological methods*, 14(1):54.
- Kornely, M. J. K. and Kateri, M. (2022). Asymptotic posterior normality of multivariate latent traits in an irt model. *Psychometrika*, 87(3):1146–1172.
- Kuhn, E. and Lavielle, M. (2004). Coupling a stochastic approximation version of emwith an mcmc procedure. *ESAIM: Probability and Statistics*, 8:115–131.
- Kyllonen, P. C. and Zu, J. (2016). Use of response time for measuring cognitive ability. *Journal of Intelligence*, 4(4):14.
- Lalor, J. P., Wu, H., and Yu, H. (2016). Building an evaluation scale using item response theory. In Su, J., Duh, K., and Carreras, X., editors, *Proceedings of the 2016 Conference on Empirical Methods in Natural Language Processing*, pages 648–657, Austin, Texas. Association for Computational Linguistics.

- Lavielle, M. and Mbogning, C. (2014). An improved saem algorithm for maximum likelihood estimation in mixtures of non linear mixed effects models. *Statistics and Computing*, 24(5):693–707.
- Li, J., Gibbons, R., and Rockova, V. (2025). Sparse bayesian multidimensional item response theory. *Journal of the American Statistical Association*, pages 1–14.
- Liang, P., Bommasani, R., Lee, T., Tsipras, D., Soylu, D., Yasunaga, M., Zhang, Y., Narayanan, D., Wu, Y., Kumar, A., Newman, B., Yuan, B., Yan, B., Zhang, C., Cosgrove, C. A., Manning, C. D., Re, C., Acosta-Navas, D., Hudson, D. A., Zelikman, E., Durmus, E., Ladhak, F., Rong, F., Ren, H., Yao, H., WANG, J., Santhanam, K., Orr, L., Zheng, L., Yuksekgonul, M., Suzgun, M., Kim, N., Guha, N., Chatterji, N. S., Khattab, O., Henderson, P., Huang, Q., Chi, R. A., Xie, S. M., Santurkar, S., Ganguli, S., Hashimoto, T., Icard, T., Zhang, T., Chaudhary, V., Wang, W., Li, X., Mai, Y., Zhang, Y., and Koreeda, Y. (2023). Holistic evaluation of language models. *Transactions on Machine Learning Research*. Featured Certification, Expert Certification.
- Liu, D. C. and Nocedal, J. (1989). On the limited memory bfgs method for large scale optimization. *Mathematical programming*, 45(1):503–528.
- Luce, R. D. (1991). *Response times: Their role in inferring elementary mental organization*. Oxford University Press.
- Maia Polo, F., Weber, L., Choshen, L., Sun, Y., Xu, G., and Yurochkin, M. (2024). tinyBenchmarks: evaluating LLMs with fewer examples. In Salakhutdinov, R., Kolter, Z., Heller, K., Weller, A., Oliver, N., Scarlett, J., and Berkenkamp, F., editors, *Proceedings of the 41st International Conference on Machine Learning*, volume 235 of *Proceedings of Machine Learning Research*, pages 34303–34326. PMLR.
- Meijer, R. R. and Nering, M. L. (1999). Computerized adaptive testing: Overview and introduction. *Applied psychological measurement*, 23(3):187–194.
- Meng, X.-B., Tao, J., and Chang, H.-H. (2015). A conditional joint modeling approach for locally dependent item responses and response times. *Journal of Educational Measurement*, 52(1):1–27.
- Reckase, M. D. (2006). 18 multidimensional item response theory. *Handbook of statistics*, 26:607–642.
- Robbins, H. and Monro, S. (1951). A stochastic approximation method. *The annals of mathematical statistics*, pages 400–407.
- Rouder, J. N., Province, J. M., Morey, R. D., Gomez, P., and Heathcote, A. (2015). The lognormal race: A cognitive-process model of choice and latency with desirable psychometric properties. *Psychometrika*, 80(2):491–513.
- Schnipke, D. L. and Scrams, D. J. (2005). Exploring issues of examinee behavior: Insights gained from response-time analyses. In *Computer-based testing*, pages 237–266. Routledge.
- Serfling, R. J. (2009). *Approximation theorems of mathematical statistics*. John Wiley & Sons.
- Snell, C. V., Lee, J., Xu, K., and Kumar, A. (2025). Scaling LLM test-time compute optimally can be more effective than scaling parameters for reasoning. In *The Thirteenth International Conference on Learning Representations*.

- van der Linden, W. J. (2007). A hierarchical framework for modeling speed and accuracy on test items. *Psychometrika*, 72(3):287–308.
- Van Der Maas, H. L., Molenaar, D., Maris, G., Kievit, R. A., and Borsboom, D. (2011). Cognitive psychology meets psychometric theory: on the relation between process models for decision making and latent variable models for individual differences. *Psychological review*, 118(2):339.
- Wainer, H., Dorans, N. J., Flaugher, R., Green, B. F., and Mislevy, R. J. (2000). *Computerized adaptive testing: A primer*. Routledge.
- Wang, C. and Xu, G. (2015). A mixture hierarchical model for response times and response accuracy. *British Journal of Mathematical and Statistical Psychology*, 68(3):456–477.
- Wei, J., Wang, X., Schuurmans, D., Bosma, M., Ichter, B., Xia, F., Chi, E. H., Le, Q. V., and Zhou, D. (2022). Chain-of-thought prompting elicits reasoning in large language models. In *Proceedings of the 36th International Conference on Neural Information Processing Systems*, NIPS '22, Red Hook, NY, USA. Curran Associates Inc.
- Xia, S., Li, X., Liu, Y., Wu, T., and Liu, P. (2025). Evaluating mathematical reasoning beyond accuracy. In *Proceedings of the AAAI Conference on Artificial Intelligence*, volume 39, pages 27723–27730.
- Zhang, H., Chen, Y., and Li, X. (2020). A note on exploratory item factor analysis by singular value decomposition. *Psychometrika*, 85(2):358–372.
- Zhuang, Y., Liu, Q., Ning, Y., Huang, W., Lv, R., Huang, Z., Zhao, G., Zhang, Z., Mao, Q., Wang, S., et al. (2023). Efficiently measuring the cognitive ability of llms: An adaptive testing perspective.

Supplementary Material

A Derivation of SAEM Algorithm

A.1 Proof of Lemma 1

In this section, we derive the complete conditional distribution of $\xi_i = (\theta_i, \tau_i)$ given Ω , \mathbf{R} , and \mathbf{T} . Due to the conditional independence structure, given Ω , \mathbf{R} , and \mathbf{T} , ξ_i 's are independent. Hence, we only need to derive the complete conditional of ξ_i . The complete conditional is,

$$\begin{aligned} P(\theta_i, \tau_i \mid \mathbf{R}_{i,:}, \mathbf{T}_{i,:}; \Omega) &\propto P(\theta_i, \tau_i; \Omega) \prod_{j=1}^J P(R_{ij} \mid \theta_i; \Omega) P(T_{ij} \mid \tau_i; \Omega) \\ &= \left[P(\theta_i; \Omega) \prod_{j=1}^J P(R_{ij} \mid \theta_i; \Omega) \right] \left[P(\tau_i \mid \theta_i; \Omega) \prod_{j=1}^J P(T_{ij} \mid \tau_i; \Omega) \right]. \end{aligned}$$

First, we focus on the conditional distribution of $P(\tau_i \mid \theta_i, \mathbf{T}_{i,:}; \Omega)$. Since $(\theta_i, \tau_i) \sim N(0, \Sigma)$, $\tau_i \mid \theta_i, \Omega \sim N(\rho\theta_i, 1 - \rho^2)$. The likelihood $P(T_{ij} \mid \tau_i; \Omega)$ is also a normal distribution. Hence, the conditional distribution is still normal.

$$\begin{aligned} P(\tau_i \mid \theta_i, \mathbf{T}_{i,:}; \Omega) &\propto p(\tau_i \mid \theta_i; \Omega) \prod_{j=1}^J P(T_{ij} \mid \tau_i; \Omega) \\ &= \exp \left\{ -\frac{1}{2(1-\rho^2)} (\tau_i - \rho\theta_i)^2 \right\} \exp \left\{ -\sum_{j=1}^J \frac{1}{2\lambda_j} (\log t_{ij} - \omega_j + \varphi_j \tau_i)^2 \right\} \\ &\propto \exp \left\{ -\frac{1}{2\check{\sigma}_\tau^{(i)2}} (\tau_i - \check{\mu}_\tau^{(i)})^2 \right\}, \end{aligned}$$

where

$$\check{\sigma}_\tau^{(i)2} = \left(\frac{1}{1-\rho^2} + \sum_{j=1}^J \frac{\varphi_j^2}{\lambda_j} \right)^{-1}, \quad \check{\mu}_\tau^{(i)} = \left(\frac{1}{1-\rho^2} + \sum_{j=1}^J \frac{\varphi_j^2}{\lambda_j} \right)^{-1} \left(\frac{\rho\theta_i}{1-\rho^2} - \sum_{j=1}^J \frac{(\log t_{ij} - \omega_j)\varphi_j}{\lambda_j^2} \right).$$

Note that $\check{\sigma}_\tau^{(i)}$ is independent of the index i . For simplicity, we will denote it as $\check{\sigma}_\tau$ from now on. Thus, the conditional distribution of τ_i is,

$$\tau_i \mid \theta_i, \mathbf{T}_{i,:}; \Omega \sim N \left(\check{\mu}_\tau^{(i)}, \check{\sigma}_\tau^2 \right).$$

Then, for the marginal distribution $P(\theta_i \mid \mathbf{R}_{i,:}; \Omega)$, note that by marginalizing out τ_i , normalizing constants containing θ_i will contribute to the marginal posterior of θ_i . In the sequel, we consider the normalizing constant "twist" $P(\theta_i; \Omega)$, and compute the twisted prior. First, for the normalizing constant concerning θ_i ,

$$\int_{\mathbb{R}} P(\tau_i \mid \theta_i; \Omega) \prod_{j=1}^J P(T_{ij} \mid \tau_i; \Omega) d\tau_i$$

$$\begin{aligned}
&\propto \int_{\mathbb{R}} \exp \left\{ -\frac{1}{2(1-\rho^2)} (\tau_i - \rho\theta_i)^2 \right\} \exp \left\{ -\sum_{j=1}^J \frac{1}{2\lambda_j} (\log t_{ij} - \omega_j + \varphi_j \tau_i)^2 \right\} d\tau_i \\
&= \exp \left\{ -\frac{\rho^2}{2(1-\rho^2)} \theta_i^2 \right\} \exp \left\{ \frac{1}{2\check{\sigma}_\tau^2} (\check{\mu}_\tau^{(i)})^2 \right\} \int_{\mathbb{R}} \exp \left\{ -\frac{1}{2\check{\sigma}_\tau^{(i)2}} (\tau_i - \check{\mu}_\tau^{(i)})^2 \right\} d\tau_i \\
&\propto \exp \left\{ -\frac{\rho^2}{2(1-\rho^2)} \theta_i^2 \right\} \exp \left\{ \frac{\rho^2}{2(1-\rho^2)^2} \left(\frac{1}{1-\rho^2} + \sum_{j=1}^J \frac{\varphi_j^2}{\lambda_j} \right)^{-1} \theta_i^2 \right. \\
&\quad \left. - \left(\frac{1}{1-\rho^2} + \sum_{j=1}^J \frac{\varphi_j^2}{\lambda_j} \right)^{-1} \left(\sum_{j=1}^J \frac{(\log T_{ij} - \omega_j) \varphi_j}{\lambda_j} \right) \frac{\rho}{1-\rho^2} \theta_i \right\}.
\end{aligned}$$

Note that

$$\frac{1}{1-\rho^2} \left(\frac{1}{1-\rho^2} + \sum_{j=1}^J \frac{\varphi_j^2}{\lambda_j} \right)^{-1} = \left(1 + (1-\rho^2) \sum_{j=1}^J \frac{\varphi_j^2}{\lambda_j} \right)^{-1} \leq 1.$$

Thus, for the normalizing constant concerning θ_i , inside the exponential, it is still a quadratic form whose quadratic term has negative coefficient. Note that $P(\theta_i; \mathbf{\Omega}) = N(0, 1)$. Denote the twisted prior of θ_i as $\tilde{\phi}(\theta_i | \mathbf{R}_{i,:}; \mathbf{\Omega})$, which is

$$\begin{aligned}
\tilde{\phi}(\theta_i | \mathbf{R}_{i,:}; \mathbf{\Omega}) &\propto \exp \left\{ -\frac{1}{2} \theta_i^2 \right\} \exp \left\{ -\frac{\rho^2}{2(1-\rho^2)} \theta_i^2 \right\} \exp \left\{ \frac{\rho^2}{2(1-\rho^2)^2} \left(\frac{1}{1-\rho^2} + \sum_{j=1}^J \frac{\varphi_j^2}{\lambda_j} \right)^{-1} \theta_i^2 \right. \\
&\quad \left. - \left(\frac{1}{1-\rho^2} + \sum_{j=1}^J \frac{\varphi_j^2}{\lambda_j} \right)^{-1} \left(\sum_{j=1}^J \frac{(\log T_{ij} - \omega_j) \varphi_j}{\lambda_j} \right) \frac{\rho}{1-\rho^2} \theta_i \right\} \\
&\propto \exp \left\{ -\frac{1-\rho^2 + \rho^2 - (1/(1-\rho^2) + \sum_j \varphi_j^2/\lambda_j)^{-1} \rho^2}{2(1-\rho^2)} \theta_i^2 \right. \\
&\quad \left. - \left(\frac{1}{1-\rho^2} + \sum_{j=1}^J \frac{\varphi_j^2}{\lambda_j} \right)^{-1} \left(\sum_{j=1}^J \frac{(\log T_{ij} - \omega_j) \varphi_j}{\lambda_j} \right) \frac{\rho}{1-\rho^2} \theta_i \right\} \\
&\propto \exp \left\{ -\frac{1}{2\sigma_\theta^{(i)2}} (\theta_i - \mu_\theta^{(i)})^2 \right\},
\end{aligned}$$

where

$$\sigma_\theta^2 = \left(\frac{1}{1-\rho^2} - \sigma_\tau^2 \frac{\rho^2}{1-\rho^2} \right)^{-1}, \quad \mu_\theta^{(i)} = \sigma_\theta^2 \left(-\sum_{j=1}^J \frac{(\log t_{ij} - \omega_j) \varphi_j}{\lambda_j^2} \right) \frac{\sigma_\tau^2 \rho}{1-\rho^2}.$$

B Proof of Identifiability

B.1 Proof of Proposition 1

This proof is similar to the proof of Proposition 3.1 in Fang et al. (2021). First, we derive the marginal distribution of R_{ij} and $\log T_{ij}$ knowing $\mathbf{\Omega}$. Let $\varepsilon_j \sim N(0, 1)$ independently for all j . Then,

for $(\theta_i, \tau_i) \sim N(0, \Sigma)$,

$$\begin{aligned}
P(R_{ij} = 1) &= \mathbb{E}_{\theta_i} [P(R_{ij} = 1 \mid \theta_i)] = \mathbb{E}_{\theta_i} \left[\mathbb{E}_{\varepsilon_j} [\mathbb{1}(\varepsilon_j \leq b_j + a_j \theta_i)] \right] \\
&= P(\varepsilon_j \leq b_j + a_j \theta_i) \\
&= P\left(\sqrt{a_j^2 + 1} \eta_j + b_j \geq 0\right) \\
&= \Psi\left(-\frac{b_j}{\sqrt{a_j^2 + 1}}\right),
\end{aligned}$$

where $\eta_j = (a_j \theta_i - \varepsilon_j) / \sqrt{a_j^2 + 1} \sim N(0, 1)$ and $\Psi(x) = 1 - \Phi(x)$ the complementary cumulative density function for a standard normal variable.

Similarly, let $\varepsilon_j \sim N(0, 1)$ independently for all j ,

$$\begin{aligned}
P(\log T_{ij} \geq \log t_{ij}) &= \mathbb{E}_{\tau_i} [P(\omega_j - \varphi_j \tau_i + \varepsilon_j \geq \log t_{ij} \mid \tau_i)] \\
&= \mathbb{E}_{\tau_i} \left[\mathbb{E}_{\varepsilon_j} [\mathbb{1}(\omega_j - \varphi_j \tau_i + \varepsilon_j \geq \log t_{ij}) \mid \tau_i] \right] \\
&= P(\omega_j - \varphi_j \tau_i + \varepsilon_j \geq \log t_{ij}) \\
&= P\left(\sqrt{\varphi_j^2 + \lambda_j} \zeta_j + \omega_j \geq \log t_{ij}\right) \\
&= \Psi\left(\frac{\log t_{ij} - \omega_j}{\sqrt{\varphi_j^2 + \lambda_j}}\right),
\end{aligned}$$

where $\zeta_j = (\varepsilon_j - \varphi_j \tau_i) / \sqrt{\varphi_j^2 + \lambda_j} \sim N(0, 1)$.

Then, we calculate the two-component marginal distribution of $(R_{i,j_1}, R_{i,j_2}), (\log T_{i,j_1}, \log T_{i,j_2}),$ and $(R_{i,j_1}, \log T_{i,j_2})$. We first compute the covariance between the following quantities.

$$\text{Cov}(\eta_{j_1}, \eta_{j_2}) = \text{Cov}\left(\frac{a_{j_1} \theta_i - \varepsilon_{j_1}}{\sqrt{a_{j_1}^2 + 1}}, \frac{a_{j_2} \theta_i - \varepsilon_{j_2}}{\sqrt{a_{j_2}^2 + 1}}\right) = \frac{a_{j_1} a_{j_2}}{\sqrt{a_{j_1}^2 + 1} \sqrt{a_{j_2}^2 + 1}}.$$

Similarly,

$$\begin{aligned}
\text{Cov}(\zeta_{j_1}, \zeta_{j_2}) &= \frac{\varphi_{j_1} \varphi_{j_2}}{\sqrt{\varphi_{j_1}^2 + \lambda_{j_1}} \sqrt{\varphi_{j_2}^2 + \lambda_{j_2}}}, \\
\text{Cov}(\eta_{j_1}, \zeta_{j_2}) &= -\frac{\rho a_{j_1} \varphi_{j_2}}{\sqrt{a_{j_1}^2 + 1} \sqrt{\varphi_{j_2}^2 + \lambda_{j_2}}}.
\end{aligned}$$

Therefore, the two-component marginal distributions are,

$$\begin{aligned}
P(R_{i,j_1} = 1, R_{i,j_2} = 1) &= P(\varepsilon_{j_1} \leq b_{j_1} + a_{j_1} \theta_i, \quad \varepsilon_{j_2} \leq b_{j_2} + a_{j_2} \theta_i) \\
&= P\left(\sqrt{a_{j_1}^2 + 1} \eta_{j_1} + b_{j_1} \geq 0, \quad \sqrt{a_{j_2}^2 + 1} \eta_{j_2} + b_{j_2} \geq 0\right) \\
&= \Psi\left(-\frac{b_{j_1}}{\sqrt{a_{j_1}^2 + 1}}, -\frac{b_{j_2}}{\sqrt{a_{j_2}^2 + 1}}, \frac{a_{j_1} a_{j_2}}{\sqrt{a_{j_1}^2 + 1} \sqrt{a_{j_2}^2 + 1}}\right),
\end{aligned}$$

where $\Psi(x_1, x_2, \rho) = P(X_1 \geq x_1, X_2 \geq x_2)$, $X_1, X_2 \sim N(0, 1)$ and $\text{Cov}(X_1, X_2) = \rho$. Similarly,

$$\begin{aligned} & P(\log T_{i,j_1} \geq \log t_{i,j_1}, \log T_{i,j_2} \geq \log t_{i,j_2}) \\ &= P\left(\sqrt{\varphi_{j_1}^2 + \lambda_{j_1}} \zeta_{j_1} + \omega_{j_1} \geq \log t_{i,j_1}, \sqrt{\varphi_{j_2}^2 + \lambda_{j_2}} \zeta_{j_2} + \omega_{j_2} \geq \log t_{i,j_2}\right) \\ &= \Psi\left(\frac{\log t_{i,j_1} - \omega_{j_1}}{\sqrt{\varphi_{j_1}^2 + \lambda_{j_1}}}, \frac{\log t_{i,j_2} - \omega_{j_2}}{\sqrt{\varphi_{j_2}^2 + \lambda_{j_2}}}, \frac{\varphi_{j_1} \varphi_{j_2}}{\sqrt{\varphi_{j_1}^2 + \lambda_{j_1}} \sqrt{\varphi_{j_2}^2 + \lambda_{j_2}}}\right), \end{aligned}$$

$$\begin{aligned} P(R_{ij} = 1, \log T_{ij} \geq \log t_{ij}) &= P\left(b_{j_1} + \sqrt{a_{j_1}^2 + 1} \eta_{j_1} \geq 0, \sqrt{\varphi_{j_1}^2 + \lambda_{j_2}} \zeta_{j_2} + \omega_{j_2} \geq \log t_{i,j_2}\right) \\ &= \Psi\left(-\frac{b_{j_1}}{\sqrt{a_{j_1}^2 + 1}}, \frac{\log t_{i,j_2} - \omega_{j_2}}{\sqrt{\varphi_{j_2}^2 + \lambda_{j_2}}}, -\frac{\rho a_{j_1} \varphi_{j_2}}{\sqrt{a_{j_1}^2 + 1} \sqrt{\varphi_{j_2}^2 + \lambda_{j_2}}}\right). \end{aligned}$$

Following this strategy, we can write out the joint distribution of $R_{i,1}, \dots, R_{i,J}, \log T_{i,1}, \dots, \log T_{i,J}$ by their pairwise covariance. For simplicity, we omit it here.

For sufficiency, suppose there are two sets of parameters Ω and Ω' following conditions in Proposition 1. Then, note that the joint distribution of \mathbf{R}_i and $\log \mathbf{T}_i$ only depends on $b_j/\sqrt{a_j^2 + 1}$, ω_j , $\sqrt{\varphi_j^2 + \lambda_j}$, $\text{Cov}(\eta_{j_1}, \eta_{j_2})$, $\text{Cov}(\zeta_{j_1}, \zeta_{j_2})$, and $\text{Cov}(\eta_{j_1}, \zeta_{j_2})$. When Ω and Ω' satisfy the set of conditions in Proposition 1, these quantities are the same. Therefore, Ω and Ω' give rise to the same joint distribution of \mathbf{R}_i and $\log \mathbf{T}_i$.

For necessity, suppose Ω and Ω' give rise to the same joint distribution of \mathbf{R}_i and $\log \mathbf{T}_i$. First, for one-component marginal distribution of R_{ij} and $\log T_{ij}$, Ω and Ω' need to satisfy,

$$\frac{b_j}{\sqrt{a_j^2 + 1}} = \frac{b'_j}{\sqrt{a_j'^2 + 1}}, \quad \frac{\log t_{ij} - \omega_j}{\sqrt{\varphi_j^2 + \lambda_j}} = \frac{\log t_{ij} - \omega'_j}{\sqrt{\varphi_j'^2 + \lambda_j'}},$$

for all $\log t_{ij} \in \mathbb{R}$. Therefore,

$$\omega_j = \omega'_j, \quad \varphi_j^2 + \lambda_j = \varphi_j'^2 + \lambda_j'. \quad (11)$$

Then, consider the two-component marginals, Ω and Ω' giving rise to the same distribution asks for the following equalities,

$$\begin{aligned} \frac{a_{j_1} a_{j_2}}{\sqrt{a_{j_1}^2 + 1} \sqrt{a_{j_2}^2 + 1}} &= \frac{a'_{j_1} a'_{j_2}}{\sqrt{a_{j_1}'^2 + 1} \sqrt{a_{j_2}'^2 + 1}}, \\ \frac{\varphi_{j_1} \varphi_{j_2}}{\sqrt{\varphi_{j_1}^2 + \lambda_{j_1}} \sqrt{\varphi_{j_2}^2 + \lambda_{j_2}}} &= \frac{\varphi'_{j_1} \varphi'_{j_2}}{\sqrt{\varphi_{j_1}'^2 + \lambda_{j_1}'} \sqrt{\varphi_{j_2}'^2 + \lambda_{j_2}'}}, \\ \frac{\rho a_{j_1} \varphi_{j_2}}{\sqrt{a_{j_1}^2 + 1} \sqrt{\varphi_{j_2}^2 + \lambda_{j_2}}} &= \frac{\rho' a'_{j_1} \varphi'_{j_2}}{\sqrt{a_{j_1}'^2 + 1} \sqrt{\varphi_{j_2}'^2 + \lambda_{j_2}'}}. \end{aligned}$$

Combining with (11), this requires

$$\frac{a_{j_1} a_{j_2}}{\sqrt{a_{j_1}^2 + 1} \sqrt{a_{j_2}^2 + 1}} = \frac{a'_{j_1} a'_{j_2}}{\sqrt{a_{j_1}'^2 + 1} \sqrt{a_{j_2}'^2 + 1}}, \quad \varphi_{j_1} \varphi_{j_2} = \varphi'_{j_1} \varphi'_{j_2}, \quad \frac{\rho a_{j_1} \varphi_{j_2}}{\sqrt{a_{j_1}^2 + 1}} = \frac{\rho' a'_{j_1} \varphi'_{j_2}}{\sqrt{a_{j_1}'^2 + 1}}.$$

Therefore, conditions in Proposition 1 are necessary.

B.2 Proof of Theorem 1

First, we show the identifiability of the probit model part. Suppose there are two sets of parameters $\boldsymbol{\Omega}$ and $\boldsymbol{\Omega}'$ that give rise to the same distribution for \mathbf{R} and $\log \mathbf{T}$. Define $\tilde{\mathbf{a}} = (\tilde{a}_1, \dots, \tilde{a}_J)$, where $\tilde{a}_j = a_j / \sqrt{a_j^2 + 1}$. Then, from Proposition 1, we have

$$\tilde{\mathbf{a}}\tilde{\mathbf{a}}^\top + \mathbf{S} = \tilde{\mathbf{a}}'\tilde{\mathbf{a}}'^\top + \mathbf{S}',$$

where $\mathbf{S} = \text{diag}\{b_j / \sqrt{a_j^2 + 1} - a_j^2 / (a_j^2 + 1)\}_{j=1}^J$ and similarly for \mathbf{S}' .

If any row of $\tilde{\mathbf{a}}$ is deleted, $\tilde{\mathbf{a}}$ still ranks 1 because there are at least 2 non-zero entries in $\tilde{\mathbf{a}}$. Then, from Theorem 5.1 in Anderson et al. (1956), $\mathbf{S}' = \mathbf{S}$ and $\tilde{\mathbf{a}}\tilde{\mathbf{a}}^\top = \tilde{\mathbf{a}}'\tilde{\mathbf{a}}'^\top$. The diagonal entries of $\tilde{\mathbf{a}}\tilde{\mathbf{a}}^\top$ and $\tilde{\mathbf{a}}'\tilde{\mathbf{a}}'^\top$ being equal implies

$$\frac{a_j^2}{a_j^2 + 1} = \frac{a_j'^2}{a_j'^2 + 1}.$$

Hence, $a_j^2 = a_j'^2$ for all $j \in [J]$. Combining with the definition of \mathbf{S} , we have $b_j = b_j'$ for all $j \in [J]$.

Additionally, by Lemma 5.1 in Anderson et al. (1956), we have

$$\frac{a_j}{\sqrt{a_j^2 + 1}} = \frac{ca_j'}{\sqrt{a_j'^2 + 1}},$$

where $c \in \{-1, 1\}$. Since $\sum_{j=1}^J a_j > 0$, c can only be 1. Therefore, $\mathbf{a} = \mathbf{a}'$.

For the parameters $\boldsymbol{\varphi}$, $\boldsymbol{\omega}$, the proof is the same as the probit model case. For $\boldsymbol{\lambda}$, since $\boldsymbol{\varphi} = \boldsymbol{\varphi}'$, $\varphi_j^2 = \varphi_j'^2$ for all $j \in [J]$, and thus $\lambda_j = \lambda_j'$ for all $j \in [J]$. For ρ , since every other parameter is identified, following Proposition 1, $\rho = \rho'$.

C Proof of APN

C.1 Assumptions

We further denote its parameter space by Θ and assume $\Theta = \bar{\mathbb{R}} \times \bar{\mathbb{R}}$, which is closed and convex. In the following, we write the log likelihood and log posterior of LaRT as

$$\begin{aligned} l^{(J)}(\theta, \tau \mid \mathbf{R}^{(J)}, \mathbf{T}^{(J)}; \boldsymbol{\Omega}) &= \sum_{j=1}^J \left[\log P(R_j^{(J)} \mid \theta; \boldsymbol{\Omega}) + \log P(T_j^{(J)} \mid \tau; \boldsymbol{\Omega}) \right], \\ \tilde{l}^{(J)}(\theta, \tau \mid \mathbf{R}^{(J)}, \mathbf{T}^{(J)}; \boldsymbol{\Omega}) &= \sum_{j=1}^J \left[\log P(R_j^{(J)} \mid \theta; \boldsymbol{\Omega}) + \log P(T_j^{(J)} \mid \tau; \boldsymbol{\Omega}) \right] - \frac{1}{2} \boldsymbol{\xi}^\top \boldsymbol{\Sigma}^{-1} \boldsymbol{\xi}, \end{aligned}$$

respectively. The corresponding Fisher information matrices for the likelihood and posterior are denoted by

$$\mathcal{I}_J(\boldsymbol{\xi}) = -\mathbb{E}_{\boldsymbol{\xi}} \left[\nabla_{\boldsymbol{\xi}}^2 l^{(J)}(\boldsymbol{\xi} \mid \mathbf{R}^{(J)}, \mathbf{T}^{(J)}; \boldsymbol{\Omega}) \right], \quad \tilde{\mathcal{I}}_J(\boldsymbol{\xi}) = -\mathbb{E}_{\boldsymbol{\xi}} \left[\nabla_{\boldsymbol{\xi}}^2 \tilde{l}^{(J)}(\boldsymbol{\xi} \mid \mathbf{R}^{(J)}, \mathbf{T}^{(J)}; \boldsymbol{\Omega}) \right].$$

We require three regularity conditions on the response-time component for establishing the asymptotic distribution, following Chang and Stout (1993); Kornely and Kateri (2022).

Assumption 1. If restricted to any compact set $K \subseteq \Theta$, $|a_j \phi(a_j \theta + b_j)|$, $|a_j^2 \phi'(a_j \theta + b_j)|$, and $|a_j^3 \phi''(a_j \theta + b_j)|$ are uniformly bounded for all $j \in \mathbb{N}$. Additionally, there exists constants $0 < d_0(K) < d_1(K) < 1$, such that for all $j \in \mathbb{N}$, we have

$$d_0(K) \leq \inf_{(j, \theta) \in \mathbb{N} \times K} \Phi(a_j \theta + b_j) \leq \sup_{(j, \theta) \in \mathbb{N} \times K} \Phi(a_j \theta + b_j) \leq d_1(K).$$

Moreover, $\sup_{j \in \mathbb{N}} \varphi_j^2 / \lambda_j \leq C < \infty$, where C is a constant.

Assumption 2. For every $(\theta, \tau) \neq (\theta_0, \tau_0)$, there is $c_1(\theta), c_2(\tau) < 0$, such that

$$\limsup_{J \rightarrow \infty} \frac{1}{J} \sum_{j=1}^J \left[\Phi(a_j \theta_0 + b_j) \log \frac{\Phi(a_j \theta + b_j)}{\Phi(a_j \theta_0 + b_j)} + \Phi(-a_j \theta_0 - b_j) \log \frac{\Phi(-a_j \theta - b_j)}{\Phi(-a_j \theta_0 - b_j)} \right] \leq c_1(\theta),$$

$$\limsup_{J \rightarrow \infty} -\frac{1}{J} \sum_{j=1}^J \frac{1}{2\lambda_j} \left[2\varphi_j(\tau - \tau_0)(\omega_j - \varphi_j \tau_0) + \varphi_j^2(\tau^2 - \tau_0^2) - 2\varphi_j \omega_j(\tau - \tau_0) \right] \leq c_2(\tau),$$

and additionally

$$\sup_{(\theta, \tau) \in \Theta \setminus B_\delta(\xi_0)} c_1(\theta) < 0, \quad \sup_{(\theta, \tau) \in \Theta \setminus B_\delta(\xi_0)} c_2(\tau) < 0,$$

for all $\delta > 0$.

Assumption 3. Assume

$$\sum_j \frac{\varphi_j^2}{\lambda_j} > 0, \quad \sum_j \frac{a_j^2 \phi(a_j \theta_0 + b_j)^2}{\Phi(a_j \theta_0 + b_j)[1 - \Phi(a_j \theta_0 + b_j)]} > 0, \quad |\rho| < 1.$$

Assumption 1 ensures that there is randomness in each entry, and the variance of the individual latent variables are bounded. Assumption 2 serves as an identifiability condition for ξ from the log posterior. That is, the ground truth ξ_0 is unique and maximizes the log posterior when $J \rightarrow \infty$. Assumption 3 makes sure the Fisher information of both the likelihood and posterior is non-degenerate. These assumptions are mild and can be satisfied in common scenarios with finite population parameters in Ω . For a more detailed discussion, one can refer to Section 6 in [Kornely and Kateri \(2022\)](#). Next, we establish the asymptotic distribution of the latent traits in Theorem 2.

C.2 Auxiliary Lemmas

First, we present there the Kolmogorov's strong law of large numbers ([Serfling, 2009](#)) for completeness.

Theorem 3 (Kolmogorov's Strong Law of Large Numbers). *Let $\{X_i\}_{i \in \mathbb{N}}$ a sequence of independent random variables with $\mathbb{E}[X_i] = \mu_i \in \mathbb{R}$ and $0 < \text{Var}(X_i) = \sigma_i^2 < \infty$. If $\sum_{i=1}^{\infty} \sigma_i^2 / i^2 < \infty$, then almost surely*

$$\frac{1}{d} \sum_{i=1}^d X_i - \frac{1}{d} \sum_{i=1}^d \mu_i \rightarrow 0,$$

for $d \rightarrow \infty$.

Denote the probabilistic model as P_{ξ_0} , where $\xi_0 = (\theta_0, \tau_0)$ the true value.

Lemma 2. Let $\{R_j, T_j\}_{j \in \mathbb{N}}$ be a set of data generated by fixed $\xi_0 = (\theta_0, \tau_0)$. Under Assumption 1 and 2,

$$\limsup_{J \rightarrow \infty} \frac{1}{J} \left[l^{(J)}(\xi \mid \mathbf{R}, \mathbf{T}) - l^{(J)}(\xi_0 \mid \mathbf{R}, \mathbf{T}) \right] \leq c_1(\theta) + c_2(\tau) < 0.$$

Proof. First, note that $l^{(J)}$ can be decomposed into two parts.

$$\begin{aligned} l^{(J)}(\xi \mid \mathbf{R}, \mathbf{T}) &= l_R^{(J)}(\theta) + l_T^{(J)}(\tau) \\ &= \sum_{j=1}^J [R_j \log \Phi(a_j \theta + b_j) + (1 - R_j) \log \Phi(-a_j \theta - b_j)] \\ &\quad - \sum_{j=1}^J \frac{1}{2\lambda_j} (\log T_{ij} + \varphi_j \tau - \omega_j)^2. \end{aligned}$$

Lemma W.2 in the web-appendix of [Kornely and Kateri \(2022\)](#) shows that

$$\limsup_{J \rightarrow \infty} \frac{1}{J} \left[l_R^{(J)}(\theta \mid \mathbf{R}) - l_R^{(J)}(\theta_0 \mid \mathbf{R}) \right] \leq c_1(\theta) < 0.$$

Then, we focus on proving $l_T^{(J)}$. Define $Z_j = [2\varphi_j(\tau - \tau_0) \log T_{ij} + \varphi_j^2(\tau^2 - \tau_0)^2 - 2\varphi_j\omega_j(\tau - \tau_0)]/2\lambda_j$, then $l_T^{(J)}(\tau \mid \mathbf{T}) - l_T^{(J)}(\tau_0 \mid \mathbf{T}) = \sum_{j=1}^J Z_j$. Since $\log T_{ij} \sim N(\omega_j - \varphi_j\tau_0, \lambda_j)$, we have

$$\mathbb{E}[Z_j] = -\frac{1}{2\lambda_j} \left[2\varphi_j(\tau - \tau_0)(\omega_j - \varphi_j\tau_0) + \varphi_j^2(\tau^2 - \tau_0^2) - 2\varphi_j\omega_j(\tau - \tau_0) \right],$$

$$\text{Var}(Z_j) = \frac{\varphi_j^2(\tau - \tau_0)^2}{\lambda_j^2} \text{Var}(\log T_j) = \frac{\varphi_j^2(\tau - \tau_0)^2}{\lambda_j} \leq (\tau - \tau_0)^2 \sup_{j \in \mathbb{N}} \frac{\varphi_j^2}{\lambda_j}.$$

Therefore, under Assumption 1,

$$\sum_{j=1}^J \frac{\text{Var}(Z_j)}{j^2} \leq (\tau - \tau_0)^2 \sup_{j \in \mathbb{N}} \frac{\varphi_j^2}{\lambda_j} \sum_{j=1}^J \frac{1}{j^2} \leq \infty.$$

Then, by Kolmogorov's strong law of large numbers, we have,

$$\frac{1}{J} \sum_{j=1}^J Z_j - \frac{1}{J} \sum_{j=1}^J \mathbb{E}_{\tau_0}[Z_j] \xrightarrow{\text{a.s.}} 0, \quad J \rightarrow \infty.$$

Under Assumption 2, $\limsup_{J \rightarrow \infty} \sum_{j=1}^J \mathbb{E}_{\tau_0}[Z_j]/J \leq c_2(\tau)$, and hence

$$\limsup_{J \rightarrow \infty} \frac{1}{J} \left[l_T^{(J)}(\tau \mid \mathbf{T}) - l_T^{(J)}(\tau_0 \mid \mathbf{T}) \right] \leq c_2(\tau) < 0.$$

□

Lemma 3. Under Assumption 1 and 2, for any $\delta > 0$, there exists a $k(\delta) < 0$ so that

$$\lim_{J \rightarrow \infty} P_{\xi_0} \left(\sup_{\xi \in \Theta \setminus B_\delta(\xi_0)} \frac{1}{J} \left(l^{(J)}(\xi \mid \mathbf{R}^{(J)}, \mathbf{T}^{(J)}) - l^{(J)}(\xi_0 \mid \mathbf{R}^{(J)}, \mathbf{T}^{(J)}) \right) < k(\delta) \right) = 1.$$

Proof. Similarly as in the proof of Lemma 2, the log likelihood can be decomposed into $l_R^{(J)}$ and $l_T^{(J)}$. The bound for $l_R^{(J)}$ is shown in Lemma 1 in Kornely and Kateri (2022). Here, we focus on the proving the following argument,

$$\lim_{J \rightarrow \infty} P_{\tau_0} \left(\sup_{\xi \in \Theta \setminus B_\delta(\xi_0)} \frac{1}{J} \left(l_T^{(J)}(\tau | \mathbf{T}^{(J)}) - l_T^{(J)}(\tau_0 | \mathbf{T}^{(J)}) \right) < k_2(\delta) \right) = 1. \quad (12)$$

Before digging into the proof, we first show combining Lemma 1 in Kornely and Kateri (2022) and (12), we obtain the desired result. For simplicity, denote A_J the series of events in Lemma 1 in Kornely and Kateri (2022), and B_J the series of events in (12). We know $\lim_{J \rightarrow \infty} P(A_J) = 1$, $\lim_{J \rightarrow \infty} P(B_J) = 1$. Then,

$$\lim_{J \rightarrow \infty} P(A_J^C \cup B_J^C) \leq \lim_{J \rightarrow \infty} P(A_J^C) + \lim_{J \rightarrow \infty} P(B_J^C) = 0.$$

Therefore, $\lim_{J \rightarrow \infty} P(A_J \cap B_J) = 1$, and we obtain the desired result.

To prove (12), we have the following decomposition. For any $\tau_i \neq \tau_0$, sufficiently small $\delta_i > 0$,

$$\begin{aligned} \frac{1}{J} \left(l_T^{(J)}(\tau | \mathbf{T}^{(J)}) - l_T^{(J)}(\tau_0 | \mathbf{T}^{(J)}) \right) &= \underbrace{\frac{1}{J} \left(l_T^{(J)}(\tau | \mathbf{T}^{(J)}) - l_T^{(J)}(\tau_i | \mathbf{T}^{(J)}) \right)}_{\alpha_1} \\ &\quad + \underbrace{\frac{1}{J} \left(l_T^{(J)}(\tau_i | \mathbf{T}^{(J)}) - l_T^{(J)}(\tau_0 | \mathbf{T}^{(J)}) \right)}_{\alpha_2}. \end{aligned}$$

For α_2 , from Lemma 2, we have

$$\limsup_{J \rightarrow \infty} \frac{1}{J} \left(l_T^{(J)}(\tau_i | \mathbf{T}^{(J)}) - l_T^{(J)}(\tau_0 | \mathbf{T}^{(J)}) \right) \leq c_2(\tau_0) < 0, \quad P_{\xi_0} - a.s.$$

In the sequel, we will bound α_1 . Consider $\tau \in \bar{B}_{\delta_i}(\tau_i)$, we first bound $\sup_{\tau \in B_{\delta_i}(\tau_i)} (l_T^{(J)}(\tau | \mathbf{T}^{(J)}) - l_T^{(J)}(\tau_i | \mathbf{T}^{(J)})/J$. Define $Z_j = [2\varphi_j(\tau - \tau_i) \log T_j + \varphi_j^2(\tau^2 - \tau_i^2) - 2\varphi_j\omega_j(\tau - \tau_i)]/(2\lambda_j)$, and $l_T^{(J)}(\tau | \mathbf{T}^{(J)}) - l_T^{(J)}(\tau_i | \mathbf{T}^{(J)}) = \sum_{j=1}^J Z_j$. Then, we bound $|\sum_{j=1}^J Z_j|/J$.

$$\frac{1}{J} \left| \sum_{j=1}^J Z_j \right| \leq \frac{1}{J} |\tau - \tau_i| \left[\underbrace{\left| \sum_{j=1}^J \frac{\varphi_j}{\lambda_j} (\log T_j - \omega_j + \varphi_j \tau) \right|}_{\beta_1} + |\tau - \tau_i| \underbrace{\left| \sum_{j=1}^J \frac{\varphi_j^2}{2\lambda_j} \right|}_{\beta_2} \right].$$

For β_1 , note that $\varphi_j(\log T_j - \omega_j + \varphi_j \tau)/\lambda_j \sim N(0, \varphi_j^2/\lambda_j)$, and $\log T_j$'s are independent. Hence,

$$\sum_{j=1}^J \frac{\varphi_j}{\lambda_j} (\log T_j - \omega_j + \varphi_j \tau) \sim N \left(0, \sum_{j=1}^J \frac{\varphi_j^2}{\lambda_j} \right).$$

By Assumption 1, $\sum_{j=1}^J \varphi_j^2/\lambda_j \leq CJ$. Then, by standard Gaussian tail bound, with probability $1 - O(J^{-8})$,

$$\beta_1 \leq 4\sqrt{CJ \log J}.$$

For β_2 , by Assumption 1,

$$\beta_2 \leq \frac{CJ}{2} |\tau - \tau_i|.$$

Moreover, $|\tau - \tau_i| \leq \delta_i$. Thus, with probability at least $1 - O(J^{-8})$,

$$\frac{1}{J} \left| \sum_{j=1}^J Z_j \right| \leq \delta_i \left[4\sqrt{\frac{C \log J}{J}} + \frac{C}{2} \delta_i \right].$$

Therefore,

$$\lim_{\delta \rightarrow 0} \sup_{\xi \in \bar{B}_\delta(\xi_i)} \frac{1}{J} \left| l_T^{(J)}(\tau | \mathbf{T}^{(J)}) - l_T^{(J)}(\tau_i | \mathbf{T}^{(J)}) \right| = 0.$$

Let $\varepsilon = -c_2(\tau_0)/2$, $\exists \delta_i > 0$ and $c_i = c_2(\tau_0)/2$,

$$\lim_{J \rightarrow \infty} P_{\xi_0} \left(\sup_{\xi \in \bar{B}_{\delta_i}(\xi_i)} \frac{1}{J} \left(l_T^{(J)}(\tau | \mathbf{T}^{(J)}) - l_T^{(J)}(\tau_i | \mathbf{T}^{(J)}) \right) < c_i < 0 \right) = 1.$$

Next, we first show the result assuming Θ is compact. Then, we extend the result to unbounded Θ . For all $\delta > 0$, $\Theta \setminus B_\delta(\xi_0)$ is still compact. For each $\delta' < \delta$, $\cup_{\xi \in \Theta \setminus B_\delta(\xi_0)} B_{\delta'}(\xi)$ is a cover for $\Theta \setminus B_\delta(\xi_0)$. Hence, there exists a finite cover $B_\delta(\xi_1), \dots, B_\delta(\xi_n)$ that form a cover of $\Theta \setminus B_\delta(\xi_0)$.

For each $B_\delta(\xi_k)$, there exists $c_k < 0$, such that

$$\lim_{J \rightarrow \infty} P_{\xi_0} \left(\sup_{\xi \in \bar{B}_{\delta_i}(\xi_i)} \frac{1}{J} \left(l_T^{(J)}(\tau | \mathbf{T}^{(J)}) - l_T^{(J)}(\tau_i | \mathbf{T}^{(J)}) \right) < c_k < 0 \right) = 1.$$

let $k = \max_{m \in [n]} c_m$, $\forall \xi \in \Theta \setminus B_\delta(\xi_0)$, by union bound

$$\begin{aligned} & \lim_{J \rightarrow \infty} P \left(\sup_{\xi \in \Theta \setminus B_\delta(\xi_0)} \frac{1}{J} \left(l_T^{(J)}(\tau | \mathbf{T}^{(J)}) - l_T^{(J)}(\tau_i | \mathbf{T}^{(J)}) \right) \geq k \right) \\ & \leq \lim_{J \rightarrow \infty} \sum_{m=1}^n P \left(\sup_{\xi \in B_{\delta'}(\xi_m)} \frac{1}{J} \left(l_T^{(J)}(\tau | \mathbf{T}^{(J)}) - l_T^{(J)}(\tau_i | \mathbf{T}^{(J)}) \right) \geq k \right) \\ & = 0. \end{aligned}$$

Hence, for every compact Θ , we have the desired result. Then, we extend the result to unbounded Θ . Define $\Theta^{(j)} = \{(\theta, \tau) \in \Theta : \delta + j \leq |\theta - \theta_0| \leq \delta + j + 1, \delta + j \leq |\tau - \tau_0| \leq \delta + j + 1\}$, $j \in \mathbb{N}$. Each $\Theta^{(j)}$ is compact and enjoys the above property. Recall the definition of $k \leq \sup_{\xi \in \Theta \setminus B_\delta(\xi_0)} c_2(\tau)/2$. Hence, let $k_j = \sup_{\xi \in \Theta^{(j)}} c_2(\tau)/2$, we have

$$\begin{aligned} \sup_{\xi \in \Theta \setminus B_\delta(\xi_0)} \frac{1}{J} \left(l_T^{(J)}(\tau | \mathbf{T}^{(J)}) - l_T^{(J)}(\tau_i | \mathbf{T}^{(J)}) \right) &= \sup_{j \in \mathbb{N}} \left(\sup_{\xi \in \Theta^{(j)}} \frac{1}{J} \left(l_T^{(J)}(\tau | \mathbf{T}^{(J)}) - l_T^{(J)}(\tau_i | \mathbf{T}^{(J)}) \right) \right) \\ &\leq \sup_{j \in \mathbb{N}} k_j \leq \sup_{\xi \in \Theta \setminus B_\delta(\xi_0)} c_2(\tau)/2 := k_2(\delta). \end{aligned}$$

Therefore,

$$\lim_{J \rightarrow \infty} P_{\xi_0} \left(\sup_{\xi \in \Theta \setminus B_\delta(\xi_0)} \frac{1}{J} \left(l_T^{(J)}(\tau | \mathbf{T}^{(J)}) - l_T^{(J)}(\tau_0 | \mathbf{T}^{(J)}) \right) < k_2(\delta) \right)$$

$$\geq \lim_{J \rightarrow \infty} P_{\xi_0} \left(\sup_{j \in \mathbb{N}} \left(\sup_{\xi \in \Theta^{(j)}} \frac{1}{J} \left(l_T^{(j)}(\tau | \mathbf{T}^{(j)}) - l_T^{(j)}(\tau_i | \mathbf{T}^{(j)}) \right) \right) \leq \sup_{j \in \mathbb{N}} k_j \right) = 1.$$

□

Lemma 4. (1) There exists $\widehat{\xi} = (\widehat{\theta}, \widehat{\tau})$ such that

$$\lim_{J \rightarrow \infty} P_{\xi_0} \left(\nabla l^{(j)}(\widehat{\theta}, \widehat{\tau} | \mathbf{R}^{(j)}, \mathbf{T}^{(j)}) = 0 \right) = 1, \quad (13)$$

$$\lim_{J \rightarrow \infty} P_{\xi_0} \left(l^{(j)}(\widehat{\theta}, \widehat{\tau} | \mathbf{R}^{(j)}, \mathbf{T}^{(j)}) = \max_{\xi \in \Theta} l^{(j)}(\xi | \mathbf{R}^{(j)}, \mathbf{T}^{(j)}) \right) = 1, \quad (14)$$

$$(\widehat{\theta}, \widehat{\tau}) \xrightarrow{P} (\theta, \tau), \quad J \rightarrow \infty. \quad (15)$$

(2) There exists $\widetilde{\xi} = (\widetilde{\theta}, \widetilde{\tau})$ such that when the log likelihood l is replaced by log posterior \widetilde{l} , the above result still holds.

Proof. (1) First, we show the existence of such solution.

Define

$$A_{\delta, \varepsilon, J} = \left\{ \sup_{\xi: \|\xi - \xi_0\| \geq \delta} \frac{1}{J} \left(l^{(j)}(\xi | \mathbf{R}^{(j)}, \mathbf{T}^{(j)}) - l^{(j)}(\xi_0 | \mathbf{R}^{(j)}, \mathbf{T}^{(j)}) \right) < \varepsilon \right\}.$$

By Lemma 3, $\lim_{J \rightarrow \infty} P_{\xi_0}(A_{\delta, \varepsilon, J}) = 1$, for all $\delta > 0$ and $\varepsilon > 0$. Given $A_{\delta, \varepsilon, J}$, the global minimum of the log likelihood must lie in $B_\delta(\xi_0)$. Next, we construct a measurable mapping from $(\{0, 1\}^J \times \mathbb{R}^J, \text{Pow}(\{0, 1\}^J) \otimes \mathcal{B}(\mathbb{R}^J)) \rightarrow (\Theta, \mathcal{B}(\Theta))$. $\text{Pow}(\{0, 1\}^J)$ denotes the power set of $\{0, 1\}^J$.

Note that $l^{(j)}(\cdot | \mathbf{R}^{(j)}, \mathbf{T}^{(j)})$ is continuous for every fixed $\mathbf{R}^{(j)}, \mathbf{T}^{(j)}$, and $l^{(j)}(\xi | \cdot)$ is continuous for every fixed ξ . Let $\Theta_\delta = \bar{B}_\delta(\xi_0) \cap \Theta$. For simplicity, we assume Θ_δ is compact. If Θ is unbounded, similar techniques as in the proof of Lemma 3 can be applied similarly, and we omit it here.

By continuity, there exists ξ^* such that,

$$l^{(j)}(\xi^* | \mathbf{R}^{(j)}, \mathbf{T}^{(j)}) = \sup_{\xi \in \Theta_\delta} l^{(j)}(\xi | \mathbf{R}^{(j)}, \mathbf{T}^{(j)}).$$

Then by Lemma W.3 in Kornely and Kateri (2022), there exists a measurable mapping $\check{\xi}_J$, such that $\xi^* = \check{\xi}_J(\mathbf{R}^{(j)}, \mathbf{T}^{(j)})$. By Lemma 3, let $\widehat{\xi}_J = \check{\xi}_J(\mathbf{R}^{(j)}, \mathbf{T}^{(j)})$, we have a sequence $\widehat{\xi}_J$ that satisfies (13) and (14).

For (15), we prove by contradiction. Suppose $\widehat{\xi}_J$ is not consistent. There exists $\varepsilon_0 > 0$, for all $\delta_0 > 0, \forall J \in \mathbb{N}, P(\|\widehat{\xi}_J - \xi_0\| > \delta_0) \geq \varepsilon_0$. Let $\widetilde{\delta} = \delta_0/2$, from Lemma 3, we have

$$\lim_{J \rightarrow \infty} P \left(\sup_{\xi \in \Theta \setminus B_{\widetilde{\delta}}(\xi_0)} \frac{1}{J} \left(l^{(j)}(\xi | \mathbf{R}^{(j)}, \mathbf{T}^{(j)}) - l^{(j)}(\xi_0 | \mathbf{R}^{(j)}, \mathbf{T}^{(j)}) \right) < c(\widetilde{\delta}) < 0 \right) = 1.$$

Let

$$A_{J, \widetilde{\delta}} = \left\{ \frac{1}{J} \left(l^{(j)}(\xi | \mathbf{R}^{(j)}, \mathbf{T}^{(j)}) - l^{(j)}(\xi_0 | \mathbf{R}^{(j)}, \mathbf{T}^{(j)}) \right) < c(\widetilde{\delta}) < 0 \right\}.$$

For all $\widetilde{\delta}$, there exists $J_0 > 0, \forall J > J_0, P(A_{J, \widetilde{\delta}}) > 1 - \widetilde{\varepsilon}$. Let $\widetilde{\varepsilon} = \varepsilon_0/2$. Since $A_{J, \widetilde{\delta}} \cap \{\|\xi_J^* - \xi_0\| > \delta_0\} = \emptyset, \{\|\xi_J^* - \xi_0\| > \delta_0\} \subseteq A_{J, \widetilde{\delta}}^c$. Thus,

$$P(\|\widehat{\xi}_J - \xi_0\| > \delta_0) \leq P(A_{J, \widetilde{\delta}}^c) < \varepsilon_0,$$

for all $J > J_0$. There is a contradiction and $\widehat{\boldsymbol{\xi}}_J$ is consistent.

(2) The key difference for $\tilde{\boldsymbol{\xi}}_J$ to satisfy (13)-(15) is to show an equivalent version of Lemma 3 for $\tilde{l}^{(J)}$. For $\tilde{l}^{(J)}$, there is the following decomposition,

$$\begin{aligned} & \frac{1}{J} \left[\tilde{l}^{(J)}(\boldsymbol{\xi} \mid \mathbf{R}^{(J)}, \mathbf{T}^{(J)}) - \tilde{l}^{(J)}(\boldsymbol{\xi}_0 \mid \mathbf{R}^{(J)}, \mathbf{T}^{(J)}) \right] \\ &= \underbrace{\frac{1}{J} \left[l^{(J)}(\boldsymbol{\xi} \mid \mathbf{R}^{(J)}, \mathbf{T}^{(J)}) - l^{(J)}(\boldsymbol{\xi}_0 \mid \mathbf{R}^{(J)}, \mathbf{T}^{(J)}) \right]}_{\alpha_1} + \underbrace{\frac{1}{J} \left[-\frac{1}{2} \boldsymbol{\xi}^\top \boldsymbol{\Sigma}^{-1} \boldsymbol{\xi} + \frac{1}{2} \boldsymbol{\xi}_0^\top \boldsymbol{\Sigma}^{-1} \boldsymbol{\xi}_0 \right]}_{\alpha_2}. \end{aligned}$$

We have shown α_1 in Lemma 3. For α_2 , since $\boldsymbol{\Sigma}$ is positive definite, $-\boldsymbol{\xi}^\top \boldsymbol{\Sigma}^{-1} \boldsymbol{\xi} / 2 \leq 0$. Because $\boldsymbol{\xi}_0$ and $\boldsymbol{\Sigma}$ are constants, $\forall \tilde{\varepsilon} > 0, \exists J_0 > 0$, for $\forall J > J_0$,

$$\sup_{\boldsymbol{\xi} \in \Theta \setminus B_{\tilde{\varepsilon}}(\boldsymbol{\xi}_0)} \frac{1}{J} \left[-\frac{1}{2} \boldsymbol{\xi}^\top \boldsymbol{\Sigma}^{-1} \boldsymbol{\xi} + \frac{1}{2} \boldsymbol{\xi}_0^\top \boldsymbol{\Sigma}^{-1} \boldsymbol{\xi}_0 \right] \leq \tilde{\varepsilon}.$$

Let $\tilde{\varepsilon} = k(\delta)/2, \tilde{k}(\delta) = k(\delta)/2$, then

$$\lim_{J \rightarrow \infty} P_{\boldsymbol{\xi}_0} \left(\sup_{\boldsymbol{\xi} \in \Theta \setminus B_{\tilde{\varepsilon}}(\boldsymbol{\xi}_0)} \frac{1}{J} \left(\tilde{l}^{(J)}(\boldsymbol{\xi} \mid \mathbf{R}^{(J)}, \mathbf{T}^{(J)}) - \tilde{l}^{(J)}(\boldsymbol{\xi}_0 \mid \mathbf{R}^{(J)}, \mathbf{T}^{(J)}) \right) < \tilde{k}(\delta) \right) = 1.$$

The following proof is the same as the proof in (1). □

Lemma 5. 1. For any $\boldsymbol{\xi} \in \Theta$, there exists $\{a_J\}_{J \in \mathbb{N}}, a_J \in [0, 1]$, such that

$$\begin{aligned} & \tilde{l}^{(J)}(\boldsymbol{\xi} \mid \mathbf{R}^{(J)}, \mathbf{T}^{(J)}) - \tilde{l}^{(J)}(\tilde{\boldsymbol{\xi}}_J \mid \mathbf{R}^{(J)}, \mathbf{T}^{(J)}) \\ &= \frac{1}{2} (\boldsymbol{\xi} - \tilde{\boldsymbol{\xi}}_J)^\top \tilde{\mathbf{H}}_J(\boldsymbol{\xi}_J^*) (\boldsymbol{\xi} - \tilde{\boldsymbol{\xi}}_J) \\ &= -\frac{1}{2} (\boldsymbol{\xi} - \tilde{\boldsymbol{\xi}}_J)^\top \left[\mathcal{I}_J(\tilde{\boldsymbol{\xi}}_J)(\mathbf{I}_2 - E_J(\boldsymbol{\xi})) + \boldsymbol{\Sigma}^{-1} \right] (\boldsymbol{\xi} - \tilde{\boldsymbol{\xi}}_J), \end{aligned}$$

where $\boldsymbol{\xi}_J^* = a_J \tilde{\boldsymbol{\xi}}_J + (1 - a_J) \boldsymbol{\xi}$, $\tilde{\mathbf{H}}_J$ is the Hessian of the log posterior, $E_J = \mathbf{I}_K + \mathcal{I}_J(\tilde{\boldsymbol{\xi}}_J)^{-1} \mathbf{H}_J(\boldsymbol{\xi}_J^*)$, and \mathbf{H}_J is the Hessian of the log likelihood.

2. For any $\varepsilon > 0$, there is $\delta > 0$, such that

$$\lim_{J \rightarrow \infty} P_{\boldsymbol{\xi}_0} \left(\sup_{\boldsymbol{\xi} \in B_\delta(\boldsymbol{\xi}_0)} \|E_J(\boldsymbol{\xi})\| < \varepsilon \right) = 1.$$

3. $\forall \varepsilon > 0, \exists \delta > 0$, for all $\boldsymbol{\xi} \in B_\delta(\boldsymbol{\xi}_0)$,

$$\begin{aligned} & \lim_{J \rightarrow \infty} P_{\boldsymbol{\xi}_0} \left((1 + \varepsilon) \tilde{V}_J(\boldsymbol{\xi}) \leq -\frac{1}{2} (\boldsymbol{\xi} - \tilde{\boldsymbol{\xi}}_J)^\top \left[\mathcal{I}_J(\tilde{\boldsymbol{\xi}}_J)(\mathbf{I}_2 - E_J(\boldsymbol{\xi})) + \boldsymbol{\Sigma}^{-1} \right] (\boldsymbol{\xi} - \tilde{\boldsymbol{\xi}}_J) \right. \\ & \quad \left. \leq (1 - \varepsilon) \tilde{V}_J(\boldsymbol{\xi}) \right) = 1, \end{aligned}$$

where $\tilde{V}_J(\boldsymbol{\xi}) = -\frac{1}{2} (\boldsymbol{\xi} - \tilde{\boldsymbol{\xi}}_J)^\top \tilde{\mathcal{I}}_J(\tilde{\boldsymbol{\xi}}_J) (\boldsymbol{\xi} - \tilde{\boldsymbol{\xi}}_J)$.

Proof. (1) The inequality directly comes from Taylor Expansion with Cauchy form of the remainder. We omit the detailed algebraic computation here.

(2) First, since

$$\frac{\partial^2 l^{(J)}}{\partial \theta \partial \tau} = 0,$$

the Hessian of the log likelihood is a diagonal matrix. Hence, the Fisher information of the log likelihood is also a diagonal matrix. By Assumption 3, because the diagonal entries are both greater than 0, the Fisher information of the log likelihood is full rank of 2. Additionally, since $\|\mathcal{I}_J(\tilde{\boldsymbol{\xi}}_J)/J\|^{-1} = 1/\sigma_{\min}(\mathcal{I}_J(\tilde{\boldsymbol{\xi}}_J)/J)$, there exists constant $C_0 > 0$, such that $\|\mathcal{I}_J(\tilde{\boldsymbol{\xi}}_J)/J\|^{-1} \leq 1/C_0$, when J is sufficiently large due to consistency of $\tilde{\boldsymbol{\xi}}_J$ shown in Lemma 4.

Hence,

$$\begin{aligned} \|E_J(\boldsymbol{\xi})\| &= \left\| \left(\frac{1}{J} \mathcal{I}_J(\tilde{\boldsymbol{\xi}}_J) \right)^{-1} \frac{1}{J} \left(\mathcal{I}_J(\tilde{\boldsymbol{\xi}}_J) + \nabla^2 l^{(J)}(\boldsymbol{\xi} \mid \mathbf{R}^{(J)}, \mathbf{T}^{(J)}) \right) \right\| \\ &\leq \left\| \frac{1}{J} \mathcal{I}_J(\tilde{\boldsymbol{\xi}}_J) \right\|^{-1} \left\| \frac{1}{J} \left(\mathcal{I}_J(\tilde{\boldsymbol{\xi}}_J) + \nabla^2 l^{(J)}(\boldsymbol{\xi} \mid \mathbf{R}^{(J)}, \mathbf{T}^{(J)}) \right) \right\| \\ &\leq \frac{1}{C_0} \left\| \frac{1}{J} \left(\mathcal{I}_J(\tilde{\boldsymbol{\xi}}_J) + \nabla^2 l^{(J)}(\boldsymbol{\xi} \mid \mathbf{R}^{(J)}, \mathbf{T}^{(J)}) \right) \right\| \\ &\leq \frac{1}{C_0} \max \{ \alpha_1, \alpha_2 \}, \end{aligned}$$

where

$$\begin{aligned} \alpha_1 &= \frac{1}{J} \left[\sum_{j=1}^J \frac{a_j^2 \phi(a_j \tilde{\theta} + b_j)}{\Phi(a_j \tilde{\theta} + b_j) [1 - \Phi(a_j \tilde{\theta} + b_j)]} - \sum_{j=1}^J \frac{a_j^2 \phi(a_j \theta + b_j)}{\Phi(a_j \theta + b_j) [1 - \Phi(a_j \theta + b_j)]} \right] \\ \alpha_2 &= \frac{1}{J} \left[\sum_{j=1}^J \frac{\varphi_j^2}{\lambda_j} - \sum_{j=1}^J \frac{\varphi_j^2}{\lambda_j} \right] = 0. \end{aligned}$$

The last inequality utilizes that both the Fisher information $\mathcal{I}_J(\tilde{\boldsymbol{\xi}}_J)$ and $\nabla^2 l^{(J)}(\boldsymbol{\xi} \mid \mathbf{R}^{(J)}, \mathbf{T}^{(J)})$ are diagonal matrices.

Since $\alpha_2 = 0$, we only need to bound α_1 . Following the same proof of Lemma 2 in Kornely and Kateri (2022), for any $\varepsilon > 0$, when J is sufficiently large, there exists $\delta > 0$, such that

$$\lim_{J \rightarrow \infty} P_{\boldsymbol{\xi}_0} \left(\sup_{\boldsymbol{\xi} \in B_\delta(\boldsymbol{\xi}_0)} \frac{1}{C_0} \alpha_1 < \varepsilon \right) = 1.$$

Therefore, the second part of Lemma 5 is proven.

(3) For the result in the third part, we first show $\forall \varepsilon > 0, \exists \delta > 0$, such that,

$$\lim_{J \rightarrow \infty} P_{\boldsymbol{\xi}_0} \left(\left| (\boldsymbol{\xi} - \tilde{\boldsymbol{\xi}}_J)^\top \mathcal{I}_J(\tilde{\boldsymbol{\xi}}_J) E_J(\boldsymbol{\xi}) (\boldsymbol{\xi} - \tilde{\boldsymbol{\xi}}_J) \right| \leq -2\varepsilon V_J(\boldsymbol{\xi}) \right) = 1,$$

where $V_J(\boldsymbol{\xi}) = -\frac{1}{2} (\boldsymbol{\xi} - \tilde{\boldsymbol{\xi}}_J)^\top \mathcal{I}_J(\tilde{\boldsymbol{\xi}}_J) (\boldsymbol{\xi} - \tilde{\boldsymbol{\xi}}_J)$

By Lemma W.5 in Kornely and Kateri (2022),

$$\left| \frac{1}{2} (\boldsymbol{\xi} - \tilde{\boldsymbol{\xi}}_J)^\top \mathcal{I}_J(\tilde{\boldsymbol{\xi}}_J) E_J(\boldsymbol{\xi}) (\boldsymbol{\xi} - \tilde{\boldsymbol{\xi}}_J) \right| \leq -\kappa(\mathcal{I}_J(\tilde{\boldsymbol{\xi}}_J)) \|E_J(\boldsymbol{\xi})\| V_J(\boldsymbol{\xi}).$$

By Assumption 3 and Lemma 4 and continuous mapping theorem, there exists C'_1 such that

$$P_{\xi_0} \left(\limsup_{J \rightarrow \infty} \kappa(\mathcal{I}_J(\tilde{\xi}_J)) \leq C'_1 \right) = 1.$$

Additionally, from (2) of this Lemma, $\|E_J(\xi)\|$ converges to 0 in probability. Hence,

$$\lim_{J \rightarrow \infty} P_{\xi_0} \left(\left| (\xi - \tilde{\xi}_J)^\top \mathcal{I}_J(\tilde{\xi}_J) E_J(\xi) (\xi - \tilde{\xi}_J) \right| \leq -2\varepsilon V_J(\xi) \right) = 1.$$

Therefore, under $\{ |(\xi - \tilde{\xi}_J)^\top \mathcal{I}_J(\tilde{\xi}_J) E_J(\xi) (\xi - \tilde{\xi}_J)| \leq -2\varepsilon V_J(\xi) \}$,

$$\begin{aligned} & -\frac{1}{2} (\xi - \tilde{\xi}_J)^\top \left[\mathcal{I}_J(\tilde{\xi}_J) (\mathbf{I}_2 - E_J(\xi)) + \Sigma^{-1} \right] (\xi - \tilde{\xi}_J) \\ & \leq V_J(\xi) + \frac{1}{2} (\xi - \tilde{\xi}_J)^\top \mathcal{I}_J(\tilde{\xi}_J) E_J(\xi) (\xi - \tilde{\xi}_J) - \frac{1}{2} (\xi - \tilde{\xi}_J)^\top \Sigma^{-1} (\xi - \tilde{\xi}_J) \\ & \leq (1 - \varepsilon) V_J(\xi) - \frac{1}{2} (\xi - \tilde{\xi}_J)^\top \Sigma^{-1} (\xi - \tilde{\xi}_J). \end{aligned}$$

Since Σ is positive definite,

$$(1 - \varepsilon) (\xi - \tilde{\xi}_J)^\top \Sigma^{-1} (\xi - \tilde{\xi}_J) \leq (\xi - \tilde{\xi}_J)^\top \Sigma^{-1} (\xi - \tilde{\xi}_J) \leq (1 + \varepsilon) (\xi - \tilde{\xi}_J)^\top \Sigma^{-1} (\xi - \tilde{\xi}_J).$$

Also, note that

$$\tilde{V}_J(\xi) = V_J(\xi) - \frac{1}{2} (\xi - \tilde{\xi}_J)^\top \Sigma^{-1} (\xi - \tilde{\xi}_J).$$

Therefore,

$$\begin{aligned} (1 - \varepsilon) \tilde{V}_J(\xi) & \geq (1 - \varepsilon) V_J(\xi) - \frac{1}{2} (\xi - \tilde{\xi}_J)^\top \Sigma^{-1} (\xi - \tilde{\xi}_J), \\ (1 + \varepsilon) \tilde{V}_J(\xi) & \leq (1 + \varepsilon) V_J(\xi) - \frac{1}{2} (\xi - \tilde{\xi}_J)^\top \Sigma^{-1} (\xi - \tilde{\xi}_J). \end{aligned}$$

Hence,

$$-\frac{1}{2} (\xi - \tilde{\xi}_J)^\top \left[\mathcal{I}_J(\tilde{\xi}_J) (\mathbf{I}_2 - E_J(\xi)) + \Sigma^{-1} \right] (\xi - \tilde{\xi}_J) \leq (1 - \varepsilon) \tilde{V}_J(\xi).$$

The other side of the inequality holds similarly. \square

Lemma 6. Let $\tilde{\Phi}(B) = P(Z \in B)$, where $Z \sim N(0, \mathcal{I})$. Under Assumption 1, 2, 3

1. For every function f that the integral $\int_{\Theta} f(\xi) \pi(\xi) d\xi$ exists, for every $\delta > 0$, we have,

$$\frac{\int_{\Theta \setminus B_\delta(\xi_0)} f(\xi) P^{(J)}(\mathbf{R}^J, \mathbf{T}^{(J)} \mid \xi) \pi(\xi) d\xi}{P^{(J)}(\mathbf{R}^{(J)}, \mathbf{T}^{(J)} \mid \tilde{\xi}_J)} \det(\tilde{\mathcal{I}}_J(\tilde{\xi}_J))^{1/2} \xrightarrow{P_{\xi_0}} 0, \quad J \rightarrow \infty.$$

2. Consider a sequence of mappings $\{G_J\}_{J \in \mathbb{N}}$, $G_J : (\Theta, \mathcal{B}(\Theta)) \rightarrow (\Theta, \mathcal{B}(\Theta))$ satisfying either of the following condition

$$\lim_{J \rightarrow \infty} P_{\xi_0} (G_J(B) \subseteq B_\delta(\xi_0)) = 1, \quad \forall \delta > 0, \quad (16)$$

$$\lim_{J \rightarrow \infty} P_{\xi_0} (G_J(B) \supseteq B_\delta(\xi_0)) = 1, \quad \forall \delta > 0, \quad (17)$$

for all bounded $B \in \mathcal{B}(\Theta)$. Then,

$$\frac{\int_{G_J(B)} P^{(J)}(\mathbf{R}^{(J)}, \mathbf{T}^{(J)} \mid \boldsymbol{\xi}) \pi(\boldsymbol{\xi}) d\boldsymbol{\xi}}{P^{(J)}(\mathbf{R}^{(J)}, \mathbf{T}^{(J)} \mid \tilde{\boldsymbol{\xi}}_J)} \det(\tilde{\mathcal{I}}_J(\tilde{\boldsymbol{\xi}}_J))^{1/2} - \tilde{\Phi} \left(\tilde{\mathcal{I}}(\tilde{\boldsymbol{\xi}}_J)^{1/2} (G_J(B) - \tilde{\boldsymbol{\xi}}_J) \right) \pi(\boldsymbol{\xi}_0) (2\pi) = o_{P_{\boldsymbol{\xi}_0}}(1).$$

Proof. **(1)** First, note that

$$\begin{aligned} & \frac{\int_{\Theta \setminus B_\delta(\boldsymbol{\xi}_0)} f(\boldsymbol{\xi}) P^{(J)}(\mathbf{R}^{(J)}, \mathbf{T}^{(J)} \mid \boldsymbol{\xi}) \pi(\boldsymbol{\xi}) d\boldsymbol{\xi}}{\pi(\tilde{\boldsymbol{\xi}}_J) P^{(J)}(\mathbf{R}^{(J)}, \mathbf{T}^{(J)} \mid \tilde{\boldsymbol{\xi}}_J)} \det(\tilde{\mathcal{I}}_J(\tilde{\boldsymbol{\xi}}_J))^{1/2} \\ &= \exp \left(\tilde{l}^{(J)}(\boldsymbol{\xi}_0 \mid \mathbf{R}^{(J)}, \mathbf{T}^{(J)}) - \tilde{l}^{(J)}(\tilde{\boldsymbol{\xi}}_J \mid \mathbf{R}^{(J)}, \mathbf{T}^{(J)}) \right) \tilde{L}_J \det(\tilde{\mathcal{I}}_J(\tilde{\boldsymbol{\xi}}_J))^{1/2}, \end{aligned}$$

where

$$\tilde{L}_J = \int_{\Theta \setminus B_\delta(\boldsymbol{\xi}_0)} \exp \left(\tilde{l}^{(J)}(\boldsymbol{\xi}_0 \mid \mathbf{R}^{(J)}, \mathbf{T}^{(J)}) - \tilde{l}^{(J)}(\tilde{\boldsymbol{\xi}}_J \mid \mathbf{R}^{(J)}, \mathbf{T}^{(J)}) \right) f(\boldsymbol{\xi}) d\boldsymbol{\xi}.$$

Since $\tilde{\boldsymbol{\xi}}_J$ is a maximum of $\tilde{l}^{(J)}$, one has

$$\exp \left(\tilde{l}^{(J)}(\boldsymbol{\xi}_0 \mid \mathbf{R}^{(J)}, \mathbf{T}^{(J)}) - \tilde{l}^{(J)}(\tilde{\boldsymbol{\xi}}_J \mid \mathbf{R}^{(J)}, \mathbf{T}^{(J)}) \right) \leq 1.$$

Hence,

$$\left| \frac{\int_{\Theta \setminus B_\delta(\boldsymbol{\xi}_0)} f(\boldsymbol{\xi}) P^{(J)}(\mathbf{R}^{(J)}, \mathbf{T}^{(J)} \mid \boldsymbol{\xi}) \pi(\boldsymbol{\xi}) d\boldsymbol{\xi}}{\pi(\tilde{\boldsymbol{\xi}}_J) P^{(J)}(\mathbf{R}^{(J)}, \mathbf{T}^{(J)} \mid \tilde{\boldsymbol{\xi}}_J)} \det(\tilde{\mathcal{I}}_J(\tilde{\boldsymbol{\xi}}_J))^{1/2} \right| \leq \left| \tilde{L}_J \det(\tilde{\mathcal{I}}_J(\tilde{\boldsymbol{\xi}}_J))^{1/2} \right|.$$

For the determinant,

$$\begin{aligned} \det(\tilde{\mathcal{I}}_J(\tilde{\boldsymbol{\xi}}_J))^{1/2} &= \sqrt{\det(\mathcal{I}_J(\tilde{\boldsymbol{\xi}}_J) + \boldsymbol{\Sigma}^{-1})} \\ &= J \sqrt{\det\left(\frac{1}{J} \mathcal{I}_J(\tilde{\boldsymbol{\xi}}_J) + \frac{1}{J} \boldsymbol{\Sigma}^{-1}\right)} \\ &\leq J \sigma_1 \left(\frac{1}{J} \mathcal{I}_J(\tilde{\boldsymbol{\xi}}_J) + \frac{1}{J} \boldsymbol{\Sigma}^{-1} \right) \\ &\leq J \left[\sigma_1 \left(\frac{1}{J} \mathcal{I}_J(\tilde{\boldsymbol{\xi}}_J) \right) + \sigma_1 \left(\frac{1}{J} \boldsymbol{\Sigma}^{-1} \right) \right], \end{aligned}$$

where the last inequality comes from Weyl's inequality. By Assumption 1, $\sigma_1(\mathcal{I}_J(\tilde{\boldsymbol{\xi}}_J)/J)$ is bounded by some constant. Since $\boldsymbol{\Sigma}$ is a constant, $\sigma_1(\boldsymbol{\Sigma}^{-1}/J) = O(1/J)$. Hence,

$$\det(\tilde{\mathcal{I}}_J(\tilde{\boldsymbol{\xi}}_J))^{1/2} = O_{P_{\boldsymbol{\xi}_0}}(J).$$

Since $\pi(\boldsymbol{\xi})$ is proper and has support over Θ ,

$$\frac{1}{P^{(J)}(\mathbf{R}^{(J)}, \mathbf{T}^{(J)} \mid \boldsymbol{\xi}_0)} \int_{\Theta \setminus B_\delta(\boldsymbol{\xi}_0)} P^{(J)}(\mathbf{R}^{(J)}, \mathbf{T}^{(J)} \mid \boldsymbol{\xi}) \pi(\boldsymbol{\xi}) d\boldsymbol{\xi} = o_{P_{\boldsymbol{\xi}_0}}(J^{-1}), \quad \forall \delta > 0.$$

For detailed discussion, one can refer to Equation (28) in [Kornely and Kateri \(2022\)](#). Additionally,

suppose there exists constant $C_f > 0$, $|f(\boldsymbol{\xi})| < C_f$ for $\boldsymbol{\xi} \in \Theta$ almost everywhere. Then,

$$\tilde{L}_J \leq C_f \left| \frac{\int_{\Theta \setminus B_\delta(\boldsymbol{\xi}_0)} P^{(J)}(\mathbf{R}^{(J)}, \mathbf{T}^{(J)} | \boldsymbol{\xi}) \pi(\boldsymbol{\xi}) d\boldsymbol{\xi}}{\pi(\boldsymbol{\xi}_0) P^{(J)}(\mathbf{R}^{(J)}, \mathbf{T}^{(J)} | \boldsymbol{\xi}_0)} \right| = o_{P_{\boldsymbol{\xi}_0}}(J^{-1}).$$

Therefore,

$$\left| \tilde{L}_J \det(\tilde{\mathcal{I}}_J(\tilde{\boldsymbol{\xi}}_J))^{1/2} \right| = o_{P_{\boldsymbol{\xi}_0}}(1).$$

(2) Let $M_{\delta,J} = B_\delta(\boldsymbol{\xi}_0)$, $U_J = \int_{M_{\delta,J}} P^{(J)}(\mathbf{R}^{(J)}, \mathbf{T}^{(J)} | \boldsymbol{\xi}) \pi(\boldsymbol{\xi}) d\boldsymbol{\xi}$.

$$\begin{aligned} & \frac{U_J \det(\tilde{\mathcal{I}}_J(\tilde{\boldsymbol{\xi}}_J))^{1/2}}{\pi(\tilde{\boldsymbol{\xi}}_J) P^{(J)}(\mathbf{R}^{(J)}, \mathbf{T}^{(J)} | \tilde{\boldsymbol{\xi}}_J)} \\ &= \frac{\det(\tilde{\mathcal{I}}_J(\tilde{\boldsymbol{\xi}}_J))^{1/2}}{\pi(\tilde{\boldsymbol{\xi}}_J)} \int_{M_{\delta,J}} \exp\left(-\frac{1}{2} (\boldsymbol{\xi} - \tilde{\boldsymbol{\xi}}_J)^\top (\mathcal{I}_J(\tilde{\boldsymbol{\xi}}_J)(\mathbf{I}_2 - E_J(\boldsymbol{\xi})) + \boldsymbol{\Sigma}^{-1}) (\boldsymbol{\xi} - \tilde{\boldsymbol{\xi}}_J)\right) d\boldsymbol{\xi}. \end{aligned}$$

From Lemma 4, for any $\varepsilon > 0$,

$$\begin{aligned} & (1 - o_{P_{\boldsymbol{\xi}_0}}(1)) \int_{M_{\delta,J}} \exp\left(-\frac{\varepsilon+1}{2} (\boldsymbol{\xi} - \tilde{\boldsymbol{\xi}}_J)^\top \tilde{\mathcal{I}}_J(\tilde{\boldsymbol{\xi}}_J) (\boldsymbol{\xi} - \tilde{\boldsymbol{\xi}}_J)\right) d\boldsymbol{\xi} \\ & \leq \int_{M_{\delta,J}} \exp\left(-\frac{1}{2} (\boldsymbol{\xi} - \tilde{\boldsymbol{\xi}}_J)^\top (\mathcal{I}_J(\tilde{\boldsymbol{\xi}}_J)(\mathbf{I}_2 - E_J(\boldsymbol{\xi})) + \boldsymbol{\Sigma}^{-1}) (\boldsymbol{\xi} - \tilde{\boldsymbol{\xi}}_J)\right) d\boldsymbol{\xi} \\ & \leq (1 + o_{P_{\boldsymbol{\xi}_0}}(1)) \int_{M_{\delta,J}} \exp\left(-\frac{1-\varepsilon}{2} (\boldsymbol{\xi} - \tilde{\boldsymbol{\xi}}_J)^\top \tilde{\mathcal{I}}_J(\tilde{\boldsymbol{\xi}}_J) (\boldsymbol{\xi} - \tilde{\boldsymbol{\xi}}_J)\right) d\boldsymbol{\xi}. \end{aligned}$$

Therefore,

$$\begin{aligned} & (1 - o_{P_{\boldsymbol{\xi}_0}}(1)) \tilde{\Phi}\left(\sqrt{1+\varepsilon} \tilde{\mathcal{I}}_J(\tilde{\boldsymbol{\xi}}_J)^{1/2} (M_{\delta,J} - \tilde{\boldsymbol{\xi}}_J)\right) (2\pi) \frac{\pi(\tilde{\boldsymbol{\xi}}_J)}{1+\varepsilon} \\ & \leq \frac{U_J \det(\tilde{\mathcal{I}}_J(\tilde{\boldsymbol{\xi}}_J))^{1/2}}{P^{(J)}(\mathbf{R}^{(J)}, \mathbf{T}^{(J)} | \tilde{\boldsymbol{\xi}}_J)} \\ & \leq (1 + o_{P_{\boldsymbol{\xi}_0}}(1)) \tilde{\Phi}\left(\sqrt{1-\varepsilon} \tilde{\mathcal{I}}_J(\tilde{\boldsymbol{\xi}}_J)^{1/2} (M_{\delta,J} - \tilde{\boldsymbol{\xi}}_J)\right) (2\pi) \frac{\pi(\tilde{\boldsymbol{\xi}}_J)}{1-\varepsilon}. \end{aligned}$$

By setting ε arbitrarily small and continuous mapping theorem from the consistency of $\tilde{\boldsymbol{\xi}}_J$, the desired result is obtained. \square

Corollary 2. Suppose a sequence $\{R_j, T_j\}_{j \in \mathbb{N}}$ generated from a fixed $\boldsymbol{\xi}_0 \in \Theta$, under Assumption 1-3, for $J \rightarrow \infty$,

$$\left(\frac{P^{(J)}(\mathbf{R}^{(J)}, \mathbf{T}^{(J)}) \det(\tilde{\mathcal{I}}_J(\tilde{\boldsymbol{\xi}}_J))^{1/2}}{P^{(J)}(\mathbf{R}^{(J)}, \mathbf{T}^{(J)} | \tilde{\boldsymbol{\xi}}_J)} \right)^{-1} \xrightarrow{P_{\boldsymbol{\xi}_0}} \frac{1}{(2\pi)\pi(\boldsymbol{\xi}_0)}.$$

Proof. By setting $G_J(B) = \mathbb{R}^2$, $J \in \mathbb{N}$, from Lemma 6, we have the desired result. \square

C.3 Proof of Theorem 2

First, we show the result for all bounded B . Then we extend to unbounded B and convergence in probability. Let $G_J(B) = \{\tilde{\mathcal{I}}_J(\tilde{\boldsymbol{\xi}}_J)^{-1/2}\mathbf{x} + \tilde{\boldsymbol{\xi}}_J : \mathbf{x} \in B\} = \tilde{\mathcal{I}}_J(\tilde{\boldsymbol{\xi}}_J)^{-1/2}B + \tilde{\boldsymbol{\xi}}_J$. Note that

$$\begin{aligned} & P(\tilde{\mathcal{I}}_J(\tilde{\boldsymbol{\xi}}_J)^{-1/2}(\boldsymbol{\xi} - \tilde{\boldsymbol{\xi}}_J) \in B \mid \mathbf{R}^{(J)}, \mathbf{T}^{(J)}) \\ &= \underbrace{\frac{\det(\tilde{\mathcal{I}}_J) \int_{G_J(B)} P^{(J)}(\mathbf{R}, \mathbf{T} \mid \boldsymbol{\xi}) \pi(\boldsymbol{\xi}) d\boldsymbol{\xi}}{P^{(J)}(\mathbf{R}^{(J)}, \mathbf{T}^{(J)} \mid \tilde{\boldsymbol{\xi}}_J)}}_{\alpha_1} \cdot \underbrace{\left(\frac{P^{(J)}(\mathbf{R}^{(J)}, \mathbf{T}^{(J)}) \det(\tilde{\mathcal{I}}_J(\tilde{\boldsymbol{\xi}}_J))}{P^{(J)}(\mathbf{R}^{(J)}, \mathbf{T}^{(J)} \mid \tilde{\boldsymbol{\xi}}_J)} \right)^{-1}}_{\alpha_2}. \end{aligned}$$

From Lemma 4, $\tilde{\boldsymbol{\xi}}_J \xrightarrow{P_{\boldsymbol{\xi}_0}} \boldsymbol{\xi}_0$, hence,

$$\|\tilde{\mathcal{I}}_J^{-1}(\tilde{\boldsymbol{\xi}}_J)\| = \frac{1}{J} \left\| \left(\frac{1}{J} \tilde{\mathcal{I}}_J(\tilde{\boldsymbol{\xi}}_J) \right)^{-1} \right\| = O_{P_{\boldsymbol{\xi}_0}} \left(\frac{1}{J} \right).$$

Thus, $\tilde{\mathcal{I}}_J^{-1}(\tilde{\boldsymbol{\xi}}_J) \xrightarrow{P_{\boldsymbol{\xi}_0}} 0$.

From Lemma 6 (2),

$$\alpha_1 \xrightarrow{P_{\boldsymbol{\xi}_0}} \tilde{\Phi} \left(\tilde{\mathcal{I}}_J(\tilde{\boldsymbol{\xi}}_J)^{-1/2}(G_J(B) - \tilde{\boldsymbol{\xi}}_J) \right) \pi(\boldsymbol{\xi}_0)(2\pi) = \tilde{\Phi}(B) \pi(\boldsymbol{\xi}_0)(2\pi), \quad J \rightarrow \infty.$$

From Corollary 2,

$$\alpha_2 \xrightarrow{P_{\boldsymbol{\xi}_0}} \frac{1}{(2\pi)\pi(\boldsymbol{\xi}_0)}.$$

Therefore, for every bounded B , combining limit distribution of α_1 and α_2 , we have the desired result. Then, for unbounded $B \in \mathcal{B}(\Theta)$, define the posterior probability measure as

$$\tilde{\Psi}_J(A) = \int_{G_J(A)} P(\boldsymbol{\xi} \mid \mathbf{R}^{(J)}, \mathbf{T}^{(J)}) d\boldsymbol{\xi}.$$

For an unbounded Borel set B , it can be written as $B = \cup_{m=1}^{\infty} B_m$, where $B_m \cap B_n = \emptyset, \forall m \neq n$, and B_m 's are bounded. Hence, for any $\varepsilon > 0$,

$$\lim_{J \rightarrow \infty} P_{\boldsymbol{\xi}_0} \left(\left| \tilde{\Psi}_J(B_m) - \Phi_2(B_m) \right| < \varepsilon \right) = 1.$$

Let $\varepsilon = 6\varepsilon'/(\pi m^2)$, we have

$$\begin{aligned} |\tilde{\Psi}_J(B) - \Phi_2(B)| &\leq \sum_{m=1}^{\infty} |\tilde{\Psi}_J(B_m) - \Phi_2(B_m)| \\ &< \sum_{m=1}^{\infty} \frac{6\varepsilon'}{\pi^2 m^2} \\ &= \varepsilon'. \end{aligned}$$

Hence, the result holds for arbitrary B .

Let $H_{d,\varepsilon}(\boldsymbol{\xi}') = P(|\tilde{\Psi}_J(B) - \Phi_2(B)| > \varepsilon \mid \boldsymbol{\xi}_0 = \boldsymbol{\xi}')$. Since $H_{d,\varepsilon} \leq 1$ uniformly, by dominated

convergence theorem,

$$\begin{aligned} \lim_{J \rightarrow \infty} P(|\tilde{\Psi}_J(B) - \Phi_2(B)| > \epsilon) &= \lim_{J \rightarrow \infty} \int_{\Theta} H_{d,\epsilon}(\boldsymbol{\xi}) d\mathcal{G}(\boldsymbol{\xi}) \\ &= \int_{\Theta} \lim_{J \rightarrow \infty} H_{d,\epsilon}(\boldsymbol{\xi}) d\mathcal{G}(\boldsymbol{\xi}) = 0, \end{aligned}$$

where $\mathcal{G}(\boldsymbol{\xi})$ is any proper probability measure on Θ . The last inequality comes from convergence in P_{ξ_0} .

D Simulation comparison with traditional SAEM implementation

This section compares the parameter estimation performance of smart initialized SAEM against traditional SAEM. The traditional SAEM is implemented with the first 20 steps with weight $\alpha_t = 1$, followed by a decay of $\alpha_t = 1/(t-20)$. The smart initialized SAEM starts with $\alpha_t = 1/t$. Parameters are generated in the same configuration as in Section 5. We conduct 200 parallel simulations.

The result is presented in Figure 10 and 11. For the probit part, there are significant outliers in the estimation of \mathbf{a} and \mathbf{b} . The outlier results from instability of the stochastic approximation E-step, when $\alpha_t = 1$. The suboptimal optimization target drives the estimate away from the true optimal region. Even excluding the outlier, the smart initialized SAEM consistently yields lower estimation error across all parameters. When the number of "burn-in" steps increases, the estimation accuracy exacerbates. We do not present the result because the many outliers when the "burn-in" steps become larger, and not ideal for presentation.

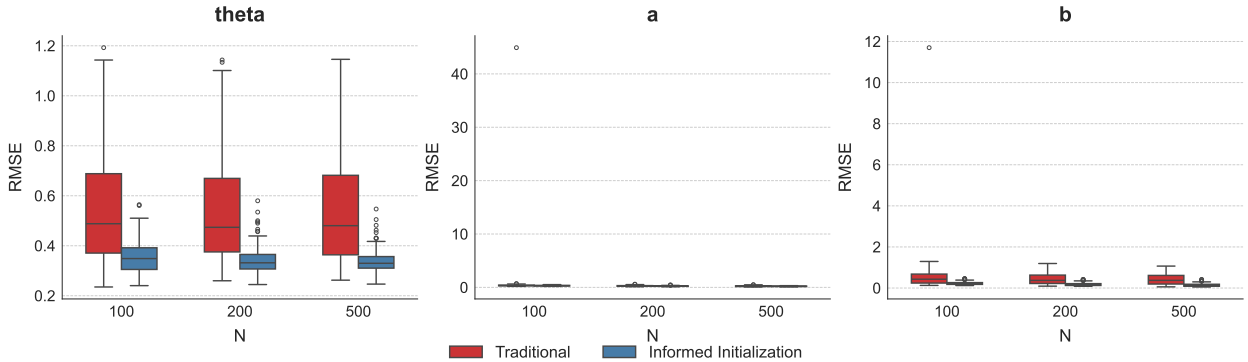


Figure 10: Comparison between smart initialized SAEM and traditional SAEM in $\boldsymbol{\theta}$, \mathbf{a} , and \mathbf{b} .

E List of Evaluated LLMs and Hyperparameters for generation

E.1 List of Evaluated LLMs

The list of models is as follows. For MATH500, we have an additional LLM google/gemma-2-27b-it.

- 01-ai/Yi-34B
- baidu/ERNIE-4.5-21B-A3B-PT
- baidu/ERNIE-4.5-21B-A3B-Thinking
- deepseek-ai/DeepSeek-R1-0528-Qwen3-8B
- deepseek-ai/DeepSeek-R1-Distill-Llama-8B
- deepseek-ai/DeepSeek-R1-Distill-Qwen-1.5B
- deepseek-ai/DeepSeek-R1-Distill-Qwen-14B
- deepseek-ai/DeepSeek-R1-Distill-Qwen-32B
- deepseek-ai/DeepSeek-R1-Distill-Qwen-7B
- dphn/dolphin-2.9.1-yi-1.5-34b
- dphn/Dolphin-Mistral-24B-Venice-Edition
- google/gemma-2b-it

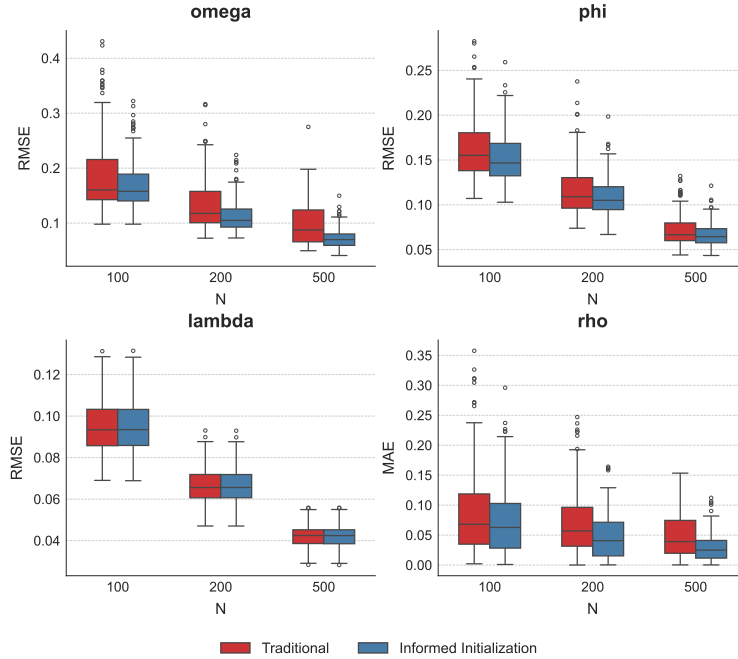


Figure 11: Comparison between smart initialized SAEM and traditional SAEM in ω , φ , λ , and ρ .

- google/gemma-3-1b-it
- google/gemma-3-1b-pt
- google/gemma-7b-it
- google/vaultgemma-1b
- HuggingFaceTB/SmolLM3-3B
- huihui-ai/Huihui-gpt-oss-20b-BF16-abliterated
- huihui-ai/Huihui-Qwen3-8B-abliterated-v2
- ibm-granite/granite-3.3-2b-instruct
- internlm/internlm2-chat-20b
- LGAI-EXAONE/EXAONE-4.0.1-32B
- LLM360/K2-Think
- meta-llama/Llama-2-7b-chat-hf
- meta-llama/Llama-2-7b-hf
- meta-llama/Llama-3.1-8B-Instruct
- meta-llama/Llama-3.2-1B
- meta-llama/Llama-3.2-1B-Instruct
- meta-llama/Llama-3.2-3B
- meta-llama/Llama-3.2-3B-Instruct
- meta-llama/Meta-Llama-3-8B
- meta-llama/Meta-Llama-3-8B-Instruct
- microsoft/Phi-3.5-mini-instruct
- microsoft/Phi-3.5-MoE-instruct
- microsoft/phi-4
- microsoft/Phi-4-mini-instruct
- microsoft/Phi-4-reasoning
- microsoft/Phi-4-reasoning-plus
- mistralai/Magistral-Small-2507
- mistralai/Magistral-Small-2509
- mistralai/Mistral-7B-Instruct-v0.1
- mistralai/Mistral-7B-Instruct-v0.2
- mistralai/Mistral-7B-Instruct-v0.3
- mistralai/Mistral-Small-3.2-24B-Instruct-2506
- mistralai/Mistral-Small-Instruct-2409
- moonshotai/Moonlight-16B-A3B
- moonshotai/Moonlight-16B-A3B-Instruct
- nvidia/AceReason-Nemotron-1.1-7B
- nvidia/AceReason-Nemotron-14B
- nvidia/Llama-3.1-Nemotron-8B-UltraLong-4M-Instruct
- nvidia/Nemotron-Research-Reasoning-Qwen-1.5B
- nvidia/NVIDIA-Nemotron-Nano-12B-v2
- nvidia/NVIDIA-Nemotron-Nano-9B-v2
- nvidia/OpenReasoning-Nemotron-1.5B
- nvidia/OpenReasoning-Nemotron-7B
- openai-community/gpt2
- openai/gpt-oss-20b
- openbmb/MiniCPM4.1-8B
- Qwen/Qwen1.5-32B
- Qwen/Qwen2-7B-Instruct
- Qwen/Qwen2.5-0.5B-Instruct
- Qwen/Qwen2.5-1.5B-Instruct
- Qwen/Qwen2.5-14B-Instruct
- Qwen/Qwen2.5-32B-Instruct
- Qwen/Qwen2.5-3B-Instruct
- Qwen/Qwen2.5-7B-Instruct
- Qwen/Qwen3-0.6B
- Qwen/Qwen3-1.7B
- Qwen/Qwen3-14B
- Qwen/Qwen3-30B-A3B
- Qwen/Qwen3-30B-A3B-Instruct-2507
- Qwen/Qwen3-30B-A3B-Thinking-2507
- Qwen/Qwen3-32B
- Qwen/Qwen3-4B
- Qwen/Qwen3-4B-Instruct-2507

- Qwen/Qwen3-4B-Thinking-2507
- Qwen/Qwen3-8B
- Qwen/QwQ-32B
- swiss-ai/Apertus-8B-Instruct-2509
- THUDM/GLM-4-9B-0414
- TinyLlama/TinyLlama-1.1B-Chat-v1.0
- zai-org/GLM-4-32B-0414

E.2 Hyperparameters and Prompts for generation

For the hyperparameters of LLMs generation, we set the temperature to be 0.5, top p 0.95, max output tokens as 10,240, and repetition penalty of 1.05. Without the repetition penalty, some LLMs will keep repeat until reach the maximum output token. Therefore, we set a mild repetition penalty such that the CoT is not repeated, and the CoT length will be a better summary of the thinking quality of an LLM.

For the prompts, we use CoT zero-shot prompting and one-shot prompting. The specific forms of the prompts are as follows. The `{problem}` provides the detailed question of the item. The one-shot example comes from a question item in MATH dataset (Hendrycks et al., 2021) that is not included in MATH500.

1. **Zero-shot Prompt:** Solve the following math problem. Be clear and concise. Problem: `"{problem}"` Provide a **step-by-step solution**. Start each step with a number followed by a period (e.g., '1.', '2.', etc.). Use basic LaTeX for mathematical expressions, such as for fractions, exponents, and variables. Avoid complex formatting. At the very end of your entire response, and only at the very end, state the final answer. This final answer must be enclosed in a single LaTeX box, like so: $\boxed{Your\ Answer}$.
2. **One-shot Prompt:** Solve the following math problem. Please think **step-by-step** to obtain the solution. Use basic LaTeX for mathematical expressions, such as for fractions, exponents, and variables. Avoid complex formatting. At the very end of your entire response, and only at the very end, state the final answer. This final answer must be enclosed in a single LaTeX box, like so: $\boxed{Your\ Answer}$.

Here is an example of how to format your response and think about solving the problem:

Example Problem: What is the sum of the two values of x for which $(x + 3)^2 = 121$?

Example Solution: Expanding the left side, we have $x^2 + 6x + 9 = 121 \Rightarrow x^2 + 6x - 112 = 0$. For a quadratic with the equation $ax^2 + bx + c = 0$, the sum of the roots is $-b/a$. Applying this formula to the problem, we have that the sum of the two roots is $-6/1 = \boxed{-6}$.

Solution: $\boxed{-6}$

— New Problem: `{problem}`.

F Supplementary Materials for Application

F.1 Behavior of One-shot Models

F.2 Ranking differences of Other Datasets

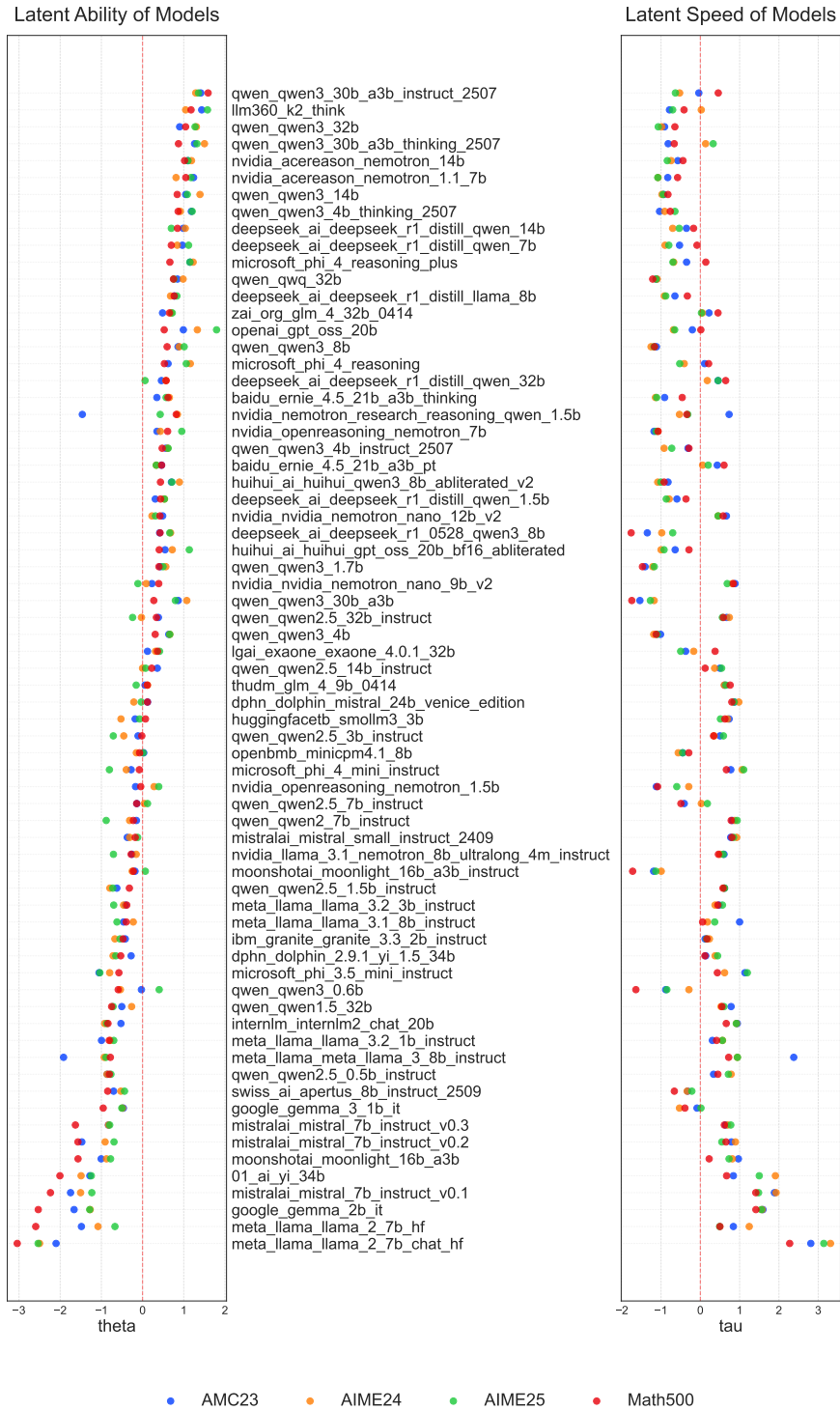


Figure 12: Estimated latent ability and latent speed of the LLMs with zero-shot prompting by LaRT. The left figure is the estimated latent ability, while the right one is the estimated latent speed. The different color represents estimated results for different benchmark datasets. As the latent ability becomes larger, the latent speed becomes smaller (longer CoT), which matches intuition.

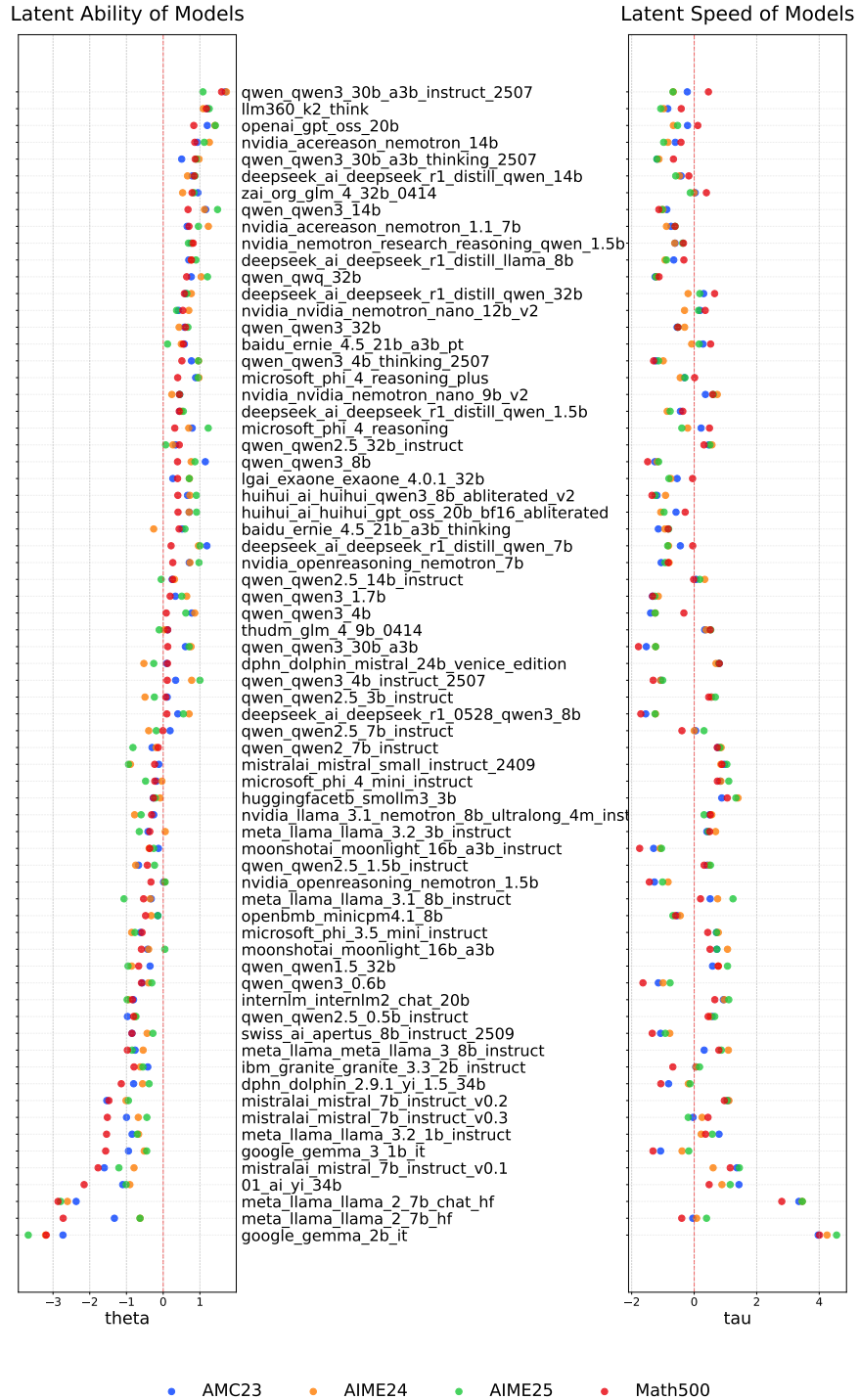


Figure 13: Estimated latent ability and latent speed of the LLMs with one-shot prompting by LaRT. The figure on the left is the estimated latent ability, while the one on the right is the estimated latent speed. The different color represents estimated results for different dataset.

Comparison of Model Rankings for MATH500

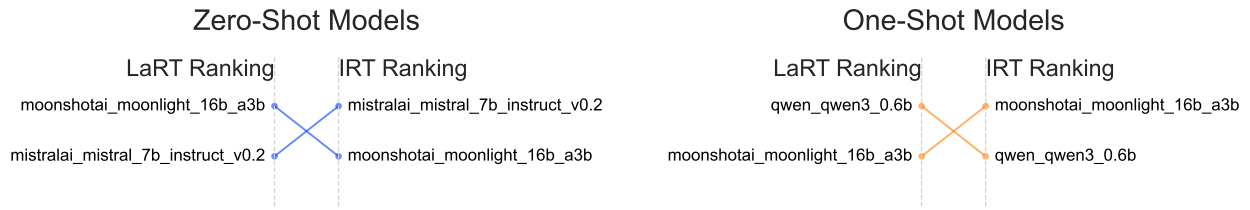


Figure 14: Differences in LLM rankings for both zero-shot models and one-shot models for MATH500. The figure on the left is for zero-shot models, and the figure on the right for one-shot models. For each of the figure, rankings by LaRT are on the left, and rankings by IRT on the right. LLMs that are higher have higher ranking. The lines connect the same models with different rankings by LaRT and IRT.

Comparison of Model Rankings for AMC23

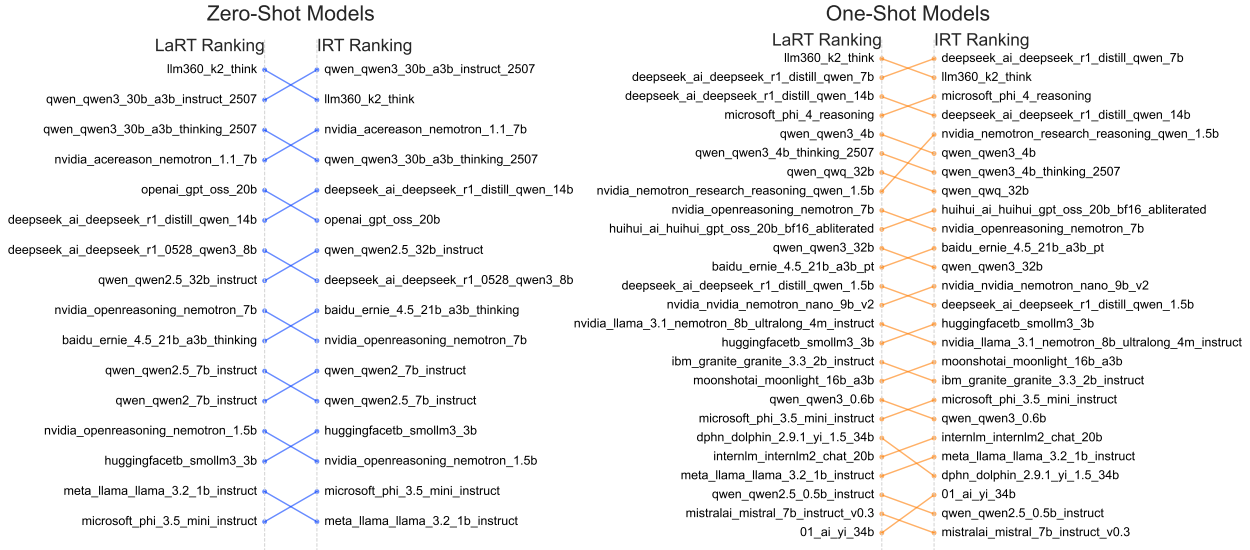


Figure 15: Differences in LLM rankings for both zero-shot models and one-shot models for AMC23. The figure on the left is for zero-shot models, and the figure on the right for one-shot models. For each of the figure, rankings by LaRT are on the left, and rankings by IRT on the right. LLMs that are higher have higher ranking. The lines connect the same models with different rankings by LaRT and IRT.

Comparison of Model Rankings for AIME24

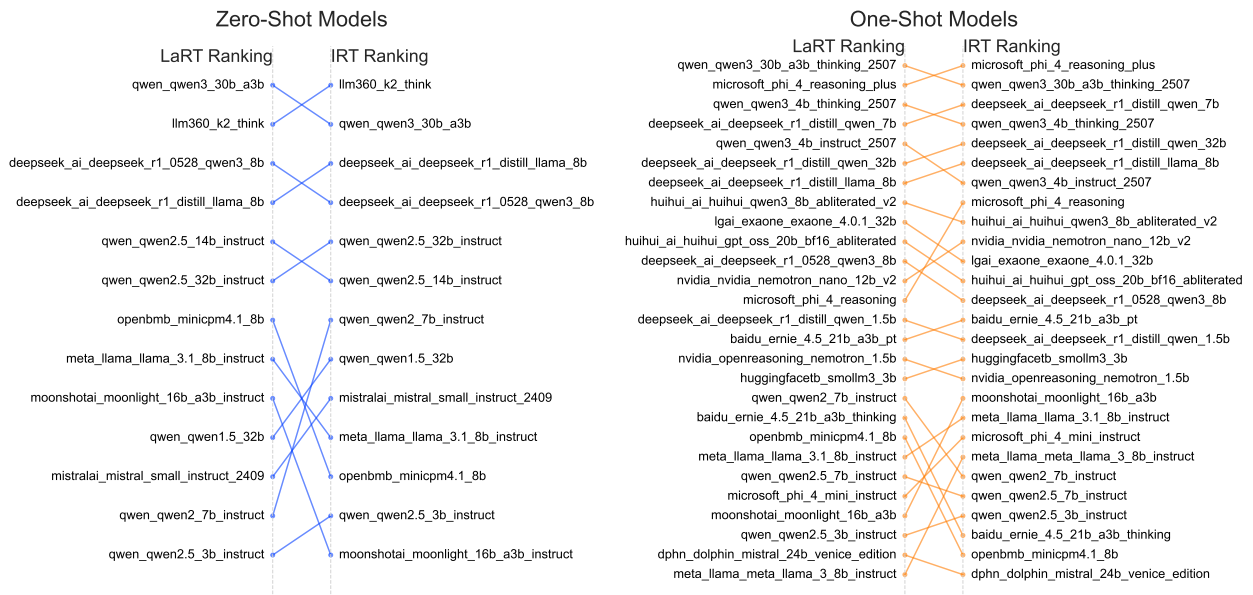


Figure 16: Differences in LLM rankings for both zero-shot models and one-shot models for AIME24. The figure on the left is for zero-shot models, and the figure on the right for one-shot models. For each of the figure, rankings by LaRT are on the left, and rankings by IRT on the right. LLMs that are higher have higher ranking. The lines connect the same models with different rankings by LaRT and IRT.